



On Gamma Ray Burst and Blazar AGN Origins of the Ultra-High Energy Cosmic Rays in Light of First Results from Auger

CHARLES D. DERMER¹

¹*Space Science Division, Code 7653, U.S. Naval Research Laboratory, Washington, D.C. 20375-5352 USA
charles.dermers@nrl.navy.mil*

Abstract: The discoveries of the GZK cutoff with the HiRes and Auger Observatories and the discovery by Auger of clustering of $\gtrsim 60$ EeV ultra-high energy cosmic rays (UHECRs) towards nearby ($\lesssim 75$ Mpc) AGNs along the supergalactic plane establishes the astrophysical origin of the UHECRs. The likely sources of the UHECRs are gamma-ray bursts and radio-loud AGNs because: (1) they are extragalactic; (2) they are sufficiently powerful; (3) acceleration to ultra-high energies can be achieved in their relativistic ejecta; (4) anomalous X-ray and γ -ray features can be explained by nonthermal hadron acceleration in relativistic blast waves; and (5) sources reside within the GZK radius. Two arguments for acceleration to UHE are presented, and limits on UHECR ion acceleration are set. UHECR ions are shown to be able to survive without photodisintegrating while passing through the AGN scattered radiation field, even if launched deep in the broad line region. UHECR injection throughout cosmic time fits the measured energy spectrum of UHECRs, at least for protons. Local UHECR proton and ion interaction and energy-loss mean free paths are calculated using an empirical fit to the extragalactic background light (EBL) at IR and optical energies. Minimum intergalactic magnetic (IGM) fields $\approx 10^{-11}$ G are derived from clustering assuming specific source origins, e.g., Cen A, nearby AGNs, or GRBs for the super-GZK CRs seen with Auger. Besides distinct cosmic-ray induced γ -ray signatures that should be observed with the *Gamma ray Large Area Space Telescope (GLAST)*, source and GZK neutrino detections and the arrival distribution of UHECR in direction and time can finally decide the sources of cosmic rays at the highest energies.

Introduction

A high-significance steepening in the UHECR spectrum at energy $E \cong 10^{19.6}$ eV was reported earlier this year by the HiRes collaboration [1], and here at the 2007 Mérida ICRC based on observations taken with the Auger Observatory [2]. This result confirms the prediction of the Greisen-Zatsepin-Kuzmin (GZK) cutoff [3, 4] in the UHECR spectrum due to photohadronic interactions of UHECRs with photons of the cosmic microwave background radiation (CMBR), and favors astrophysical bottom-up vs. particle physics top-down scenarios for the UHECRs, provided that sources are found within the GZK radius.

At the same time, Auger data shows [5] evidence for mixed composition with substantial ion content in UHECRs with energies as high as a *few* $\times 10^{19}$ eV, based on studies of the depth of shower maxima. With hybrid fluorescence detectors and shower counters, Auger provides the strongest evi-

dence yet for metals in the UHECRs, possibly with mean atomic mass $\langle A \rangle \sim 8 - 26$, significantly different from pure proton and pure Fe composition. This result depends on the accuracy of the nuclear interaction physics used to model showers, but points to the importance of nuclei in the UHECRs, and the meaning of this for GZK physics [6, 7, 8].

The GZK radius of a proton with energy $E = E_{par} = 10^{20} E_{20}$ eV can be estimated by noting that the product of the cross section and the inelasticity in a pion-producing reaction is $K_{\phi\pi}\sigma_{\phi\pi} \approx 70 \mu\text{b}$ [9], so that the photopion energy-loss pathlength $r_{\phi\pi}(E)$ is given by $n_{ph}(E)(K_{\phi\pi}\sigma_{\phi\pi})r_{\phi\pi}(E) = 1$, where $n_{ph}(E)$ is the E -dependent number density of photons above the pion-production threshold.

There are ≈ 400 CMBR photons per cm^3 at the present epoch, and ions with Lorentz factor $\gamma = E/Am_p c^2$ satisfying $\gamma(h\nu/m_e c^2) \gtrsim 2m_\pi/m_e \cong$

500 will interact with most of the photons of the CMBR. The mean dimensionless photon energy in the CMBR is $h\langle\nu\rangle/m_e c^2 \cong 2.70 k_B T_{\text{CMBR}}/m_e c^2 \cong 1.3 \times 10^{-9}$, noting that $T_{\text{CMBR}} = 2.72$ K at the present epoch; hence UHECR protons with Lorentz factor $\gamma \gtrsim 4 \times 10^{11}$, or $E \gtrsim 4 \times 10^{20}$ eV will have a photo-pion energy-loss pathlength $r_{\phi\pi}(E \gtrsim 4 \times 10^{20} \text{ eV}) \approx 12$ Mpc. By considering the number of photons above threshold in a blackbody distribution, the energy-loss mean free path of an UHECR proton with energy E is found to be

$$r_{\phi\pi}(E_{20}) \cong \frac{13.7 \exp[4/E_{20}]}{[1 + 4/E_{20}]} \text{ Mpc}. \quad (1)$$

Figure 1 shows the photopion energy-loss pathlength from eq. (1) for cosmic-ray protons interacting with CMBR photons, in comparison with a more detailed calculation [10].

Auger results show a mixed UHECR composition extending from $\approx 4.5 \times 10^{17} \text{ eV} - 4.5 \times 10^{19} \text{ eV}$, with an indication of increased average mass at the highest energy datum [5]. The ionic content of the UHECR provides new information to understand UHECR source properties, especially if the distribution of atomic mass A can be obtained with better statistics.

Figure 1 shows expansion, photohadronic, and total energy-loss mean free paths (MFPs) for p and Fe on the CMBR. Calculations of photopair losses follow [11]. The photopion loss calculation can be extended to ions of atomic mass A and charge Z by assuming that the photopion cross-section times inelasticity is at most $= A^{2/3} K_{\phi\pi} \sigma_{\phi\pi}$ above threshold. The photopion energy-loss rate of Fe with this assumption for the product of the inelasticity and cross section is shown in Figure 1. Because of the greater mass of Fe than p, far fewer photons are available for photopion interactions than with protons carrying the same energy, so that the corresponding GZK photopion radius is much larger.

Ions are in addition subject to losses due to photonuclear interactions that can break up nuclei (for example, via the giant dipole resonance). The photodisintegration loss length for Fe in the CMBR at $z \ll 1$, calculated from model fits to photohadronic cross section data [12, 13], is plotted in Figure 1.

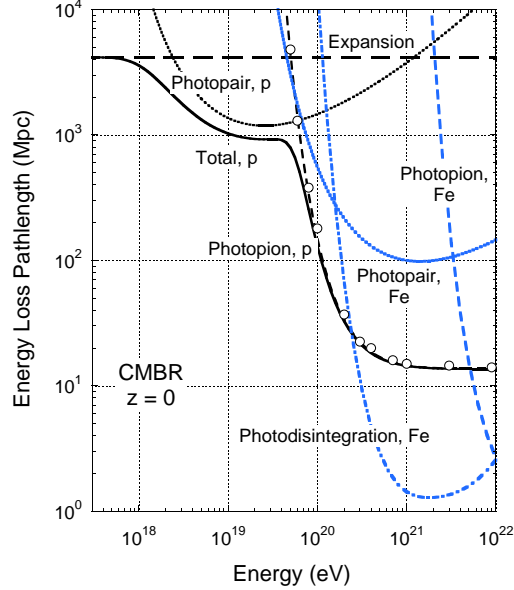


Figure 1: Energy-loss mean-free path for UHECR protons (black) and Fe ions (gray) in the CMBR at $z = 0$, as a function of total particle energy. The short-dashed black curve give the analytical approximation for the UHECR proton photopion energy-loss pathlength, eq. (1), in comparison with the numerical results, shown by open circles [10]. Numerical results for the photopair energy-loss pathlength of UHECR protons and Fe are shown by the dotted curves. The gray dot-dashed curve gives the photodisintegration energy-loss curve of Fe. Expansion losses are shown by the long-dashed line, with $c/H_0 = 4170$ Mpc.

UHECR Fe is seen to have a comparable GZK-type cutoff, but here at $\approx 2 \times 10^{20}$ eV, with photopair losses playing a minor role.

A realistic calculation of UHECR ion spectra in the evolving background radiation fields must follow a reaction pathway using Monte Carlo techniques, with the actual effective energy-loss pathlength taking into account the EBL intensity contributed by stars and black holes, then sometimes reprocessed through dust and gas. The exact form of the EBL intensity between ≈ 1 and 100μ is poorly known, but can be constrained by empirical galaxy SEDs and γ -ray observations.

From the curves shown in Figure 1, we see that for either UHECR protons or Fe ions, the sources

of $E \gtrsim 10^{20}$ eV cosmic rays must be found within a few hundred Mpc, and the 3×10^{20} eV cosmic ray detected by the Fly's Eye [14] must have originated from a source within a few tens of Mpc. Both gamma-ray bursts (GRBs) and radio-loud active galactic nuclei (AGNs¹) satisfy this requirement. Besides the availability of extragalactic sources within tens of Mpc, several other conditions must also be met, including

1. sufficient power to make the UHECRs at the observed intensity;
2. a plausible mechanism to accelerate particles to $\gtrsim 10^{20}$ eV energies; and
3. a model that can reproduce the observed UHECR spectrum, consistent with astronomical properties of the sources.

The Auger clustering observations [15] suggest new calculations to determine the intergalactic medium (IGM) magnetic field. If the 2 (out of 27 total) UHECRs with arrival directions within 3° of Cen A are hypothesized to originate from Cen A, then lower values of the mean IGM field can be derived, $\gtrsim 10^{-10}$ G, between us and Cen A, and $\gtrsim 10^{-11}$ G for sources at 75 Mpc. The clustering observations and the GZK length are tightly coupled concepts [16], as is established with the Auger data. Here we give new proton and ion energy loss calculations after revisiting the problem of the EBL.

The Auger discovery [15] that the arrival directions of > 56 EeV are correlated with nearby, $\lesssim 75$ Mpc AGNs, in particular, 2 cosmic rays within 3° of Centaurus A, does not mean that AGNs are the sources of UHECRs, any more than O and B stars correlated with galactic γ -ray sources mean that cosmic rays are accelerated by high-mass stars [17]. Long duration GRBs trace sites of active star formation, and may be correlated to AGN activity. AGNs trace the local matter distribution due to structure formation, as do radio galaxies and GRBs, or for that matter clusters of galaxies and radio-quiet Sy AGN. Here we make the case for GRB and radio-loud AGN/blazars as the sources of the UHECRs. UHECR ion acceleration in clusters of galaxies could also make a contribution at $\lesssim 10^{19}$ eV, or from dim quasars [18], but this anal-

ysis forces us to reject UHECR origin from radio-quiet AGNs.

Effects of UHECR hadron acceleration can be varied, including anomalous γ -ray emissions and characteristic behaviors of GRB X-ray light curves. Detection of high-energy neutrinos from hadronic interactions at the sources will provide the most definitive evidence for the presence of UHECRs [19]. Detection of cosmogenic GZK neutrinos from the decay of pions formed in GZK interactions with CMBR photons gives a calorimetric measure of UHECR power throughout cosmic time, with a characteristic spectrum imprinted by production and propagation effects. ANITA and successor Askaryan-effect detectors should soon be able to constrain a long-duration GRB model of UHECRs, if they were protons. Metals in the composition of UHECRs change the spectral predictions, as well as the GZK neutrino predictions [20, 21]. The result of UHECR ions vs. protons is mainly to enhance neutron β -decay neutrinos but not significantly change the \sim EeV neutrino flux.

Joint analysis of UHECR spectral, composition, and directional information, now given most accurately with the hybrid Auger, with neutrino and γ -ray data from GLAST, AGILE, and the ground-based air and water Cherenkov detectors, should lead to a definitive solution to the problem of UHECR origin. A black hole origin is explored here. Crucial to progress are the advances in detector capabilities and instrumentation, multiwavelength observations and multi-disciplinary analyses.

Extragalactic Origin and Source Energetics

The Larmor radius of an UHECR ion [22] is

$$r_L = \frac{E}{QB} \cong 1.1 \frac{(E/10^{19} \text{ eV})}{(Z/10)B(\mu\text{G})} \text{ kpc} \\ \cong 600 \frac{(E/6 \times 10^{19} \text{ eV})}{(Z/10) B_{-11}} \text{ Mpc}, \quad (2)$$

where $B = 10^{-11} B_{-11}$ G is the mean magnetic field in which the ion propagates. A significant

1. Blazars are radio-loud AGNs viewed along the jet axis; here the two terms are used interchangeably.

Table 1: UHECR Source Emissivity

E (eV)	J_{24}^a	r_{tot} (Mpc)	$\dot{\mathcal{E}}_{44}$
10^{20}	0.6	140	0.4
$10^{19.5}$	1.8	900	0.4
10^{19}	1.4	1000	0.8
$10^{18.5}$	1.0	1700	1.2
10^{18}	2.0	$\cong 4000$	3.0

^aFrom Auger data [2].

anisotropy in the arrival directions of UHECRs with energies exceeding $\approx 10^{19}$ eV might be expected from Galactic sources along the Galactic plane or towards the Galactic Center, even if they were composed primarily of Fe ($Z = 26$), because any likely source class (pulsars, supernovae, microquasars, high mass stars) would be confined to the thick disk of the Galaxy. HiRes found no evidence for small-scale or large-scale clustering [23]. The Auger discovery [15] of UHECR clustering along the supergalactic plane, anticipated in analysis of AGASA, Haverah Park, and Yakutsk data [16], immediately rules out a galactic origin of the UHECRs.

We now calculate the emissivity $\dot{\mathcal{E}}$ required to power UHECRs, assuming (incorrectly) that UHECRs are protons that suffer expansion cooling and photopion and photopair losses on the CMBR. The Auger observations [2] of the spectrum of UHECRs, written in the form $J_{24} = E^3 J / (10^{24} \text{ eV}^2 \text{ m}^{-2} \text{ s}^{-1} \text{ sr}^{-1})$, where J is the UHECR number intensity, implies that the energy density of UHECRs with energy E_{20} is $u_{uhec} \cong 6.7 \times 10^{-22} J_{24} / E_{20}$ ergs cm^{-3} . Using the energy-loss pathlengths shown in Fig. 1 gives² $\dot{\mathcal{E}} = u_{uhec} / t_{tot} = cu_{uhec} / r_{tot}$, so

$$\dot{\mathcal{E}} \left(\frac{\text{ergs}}{\text{Mpc}^3 \cdot \text{yr}} \right) = \frac{6.0 \times 10^{45}}{r_{tot}(\text{Mpc})} \frac{J_{24}}{E_{20}}. \quad (3)$$

The sources of UHECRs with energy $\approx 10^{20} E_{20}$ eV must provide an emissivity $\dot{\mathcal{E}}_{44}$, in units of 10^{44} ergs $\text{Mpc}^{-3} \text{ yr}^{-1}$, given by the values shown in Table 1.

The required emissivity, from Table 1 using the Auger intensity, is $\approx \text{few} \times 10^{44}$ ergs $\text{Mpc}^{-3} \text{ yr}^{-1}$ for $E \gtrsim 10^{19}$ eV, and $\approx 10^{45}$ ergs $\text{Mpc}^{-3} \text{ yr}^{-1}$ for $E \gtrsim 10^{18}$ eV. Between 10^{18} eV and 10^{20} eV, the increased energy density in UHECRs at

the lower energies of this range is balanced by the larger energy-loss length, thereby making the injection emissivity roughly constant with energy. At $E \lesssim 10^{18}$ eV, the emissivity increases roughly proportional to energy because the energy-loss pathlength is approximately equal to the Hubble radius at 10^{18} eV, and $E^2 J \propto 1/E$ at these energies.

Classical long duration GRBs have a volume- and time-averaged emissivity in the X-ray/soft γ ray (“ X/γ ”) band comparable to this value, a coincidence first noted by Vietri [24] and Waxman [25]. We can reproduce this estimate by noting that the average $\gtrsim 20$ keV fluence of BATSE (the Burst and Transient Source Experiment (BATSE) on the *Compton Observatory*) GRBs is $\approx 10^{-5}$ ergs cm^{-2} [26], and that there are about 500 long-duration BATSE GRBs over the full sky per year [27], giving an average GRB flux of $\approx 10^{-2}$ ergs $\text{cm}^{-2} \text{ yr}^{-1}$.³ BATSE GRBs are, on average, at redshift $z \approx 1$ (Hubble radius $R_H \cong 4200$ Mpc), so that the $\gtrsim 20$ keV emissivity of long duration GRBs is

$$\dot{\mathcal{E}}_{GRB} \approx \frac{4\pi R_H^2 \times 10^{-2} \text{ ergs cm}^{-2} \text{ yr}^{-1}}{4\pi R_H^3/3} \cong 7 \times 10^{43} \text{ ergs Mpc}^{-3} \text{ yr}^{-1}, \quad (4)$$

in rough agreement with the UHECR emissivity requirements shown in Table 1.

Two assumptions (at least) underlay this estimate: One is that an average emissivity can apply to the peculiar emissivity of the local $\lesssim 100$ Mpc sphere that we inhabit. Greater GRB activity at $z \gtrsim 1$ compared to the present epoch means that there would be fewer sources within the GZK radius [28]. On the other hand, additional classes of GRB sources, in particular, the X-ray flashes or the low luminosity GRBs [29], can provide a substantial addition to the emissivity. Wang et al. (2007) [30] estimate a local emissivity $\dot{\mathcal{E}} \approx 250 \times 10^{44}$ ergs $\text{Mpc}^{-3} \text{ yr}^{-1}$ in the kinetic output of nearby low-luminosity GRB hypernovae (which exceeds

2. This is the *proton* GZK radius. Ion energy-loss pathlengths are calculated later in the paper.

3. González (private communication, 2003), calculates a total fluence per year of 0.63×10^{-2} ergs cm^{-2} for 1293 GRBs in the 4th BATSE catalog, including GRBs of both long- and short-duration, considering 666 GRBs/yr full sky, implying a bolometric average energy density $\lesssim 10^{-20}$ ergs cm^{-3} of GRB light.

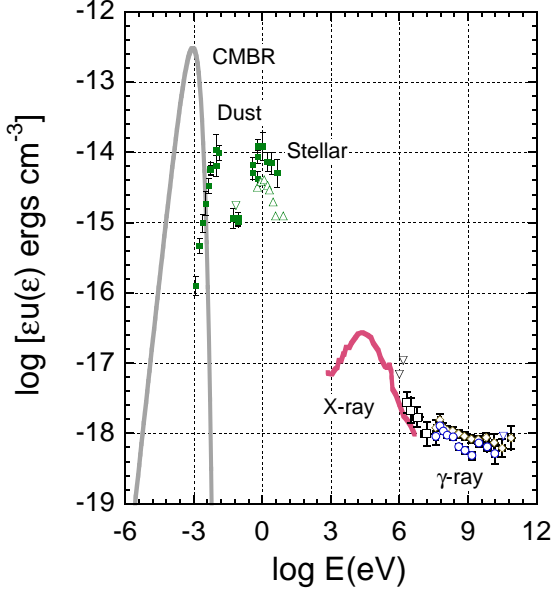


Figure 2: Intensity of extragalactic background light from the microwave through the γ -rays, with components as labeled.

the emissivity in observed γ rays). A further assumption is that there is comparable energy injected in UHECRs as detected in electromagnetic radiation. This could well be wrong. A large, $\approx 30 - 100$, baryon loading is required if long duration BATSE/Beppo-SAX/GBM-type GRBs are the sources of UHECRs [31].

A similar emissivity estimate for blazar AGNs can be made on the basis of the unresolved/diffuse extragalactic γ radiation (DEGR) observed with the Energetic Gamma-Ray Experiment Telescope (EGRET) on the *Compton Observatory* [32, 33] (see Fig. 2). Between ≈ 100 MeV and ≈ 100 GeV, the “ νF_ν ” intensity $\epsilon I_\epsilon \approx 1.5 \text{ keV cm}^{-2} \text{ s}^{-1} \text{ sr}^{-1}$, so that the diffuse γ -ray energy flux received here at Earth is $\approx 0.5 \text{ erg cm}^{-2} \text{ yr}^{-1}$. Because blazar AGNs comprise the largest number of identified EGRET sources, they undoubtedly make up a large fraction of this radiation, with estimates ranging from $\approx 20\%$ to nearly 100% .

It is important here to distinguish between the nearly lineless BL Lac objects and the flat spectrum radio quasars (FSRQs) with strong broad, optical emission lines. The BL Lac objects detected

at γ -ray energies are at mean redshift $\langle z \rangle \approx 0.3$, whereas the FSRQs detected with EGRET are at $\langle z \rangle \approx 1$. The BL Lac and FSRQ contributions to the DEGR are found [34] from model fits to the redshift and peak flux γ -ray data to contribute at the $\sim 5\%$ and $\sim 15\%$ of the total diffuse γ -ray intensity, respectively.

Following the reasoning leading to eq. 4, the mean emissivity in γ rays is $\dot{\epsilon}_{BL\text{ Lac}} \approx 10^{45} \text{ ergs Mpc}^{-3} \text{ yr}^{-1}$ for BL Lac objects, and $\dot{\epsilon}_{FSRQ} \approx 6 \times 10^{44} \text{ ergs Mpc}^{-3} \text{ yr}^{-1}$ for FSRQs. On the basis of energetics arguments, both FSRQs and BL Lacs appear to have sufficient energy to power the UHECRs. The more powerful FSRQs are, however, rare in our local vicinity, so that average emissivity becomes a mistaken concept. The nearest high luminosity FR II radio galaxies associated with FSRQs are at $z \approx 0.1$; the FR II radio galaxy Cygnus A has $z \approx 0.056$, so is ≈ 250 Mpc distant, and is far outside the GZK radius for a 10^{20} eV proton.

By comparison, many low-luminosity FR I radio galaxies associated with BL Lac objects are found nearby. For example, Centaurus A and M87 are ≈ 4 and ≈ 16 Mpc distant, respectively. These FR Is have lower jet power than the powerful FR IIs. This makes it more difficult to accelerate protons to ultra-high energies, though not heavy ions, as we now show.

Acceleration to Ultra-High Energies

Acceleration in relativistic blast waves can proceed through a number of mechanisms. First-order shock Fermi acceleration, analogous to the standard particle acceleration mechanism in supernova remnant shocks, is the obvious process [35]. But acceleration of particles to ultra-high energies through first-order processes at a relativistic external shock encounters kinematic difficulties to reach ultra-high energies [36, 37]. When particles diffuse upstream from the shock, the shock overtakes the particles before they can change their direction by more than an angle $\approx 1/\Gamma$, where Γ is the Lorentz factor of the blast wave. This prevents the particle from increasing its energy by more than a factor ≈ 2 in each cycle following the first particle capture by the blast wave. Even so, acceleration

to UHE through first-order relativistic shock acceleration can take place if the surrounding medium is strongly magnetized, as could be the case in the winds of a massive Wolf-Rayet progenitor. If the colliding shells of blazars and GRBs are sufficiently magnetized, first-order processes can also apparently accelerate protons to UHEs [25].

Here we present two arguments showing that UHEs can be achieved in the relativistic shocks of GRBs and blazars. The first considers stochastic acceleration in the external shock of a GRB or blazar, and the second considers general source power requirements [38] for particle acceleration in GRBs, blazars, or other candidate UHECR sources.

A. Stochastic Acceleration in the Blast Wave Shell

Second-order processes in an external shock of a blast wave can be shown to permit hadronic acceleration to ultra-high energies, in comparison with radiative and expansion losses and escape [39]. Using parameters appropriate to a GRB, consider a blast wave with apparent isotropic energy release $E_0 = 10^{54} E_{54}$ ergs, (initial) coasting Lorentz factor $\Gamma_0 = 300 \Gamma_{300}$, and external medium density $n_0 = 100 n_2 \text{ cm}^{-3}$. The comoving blast-wave volume for a spherically symmetric explosion at distance x from the center of the explosion is

$$V' = 4\pi x^2 \Delta', \quad (5)$$

where primes refer to the comoving frame, and the shell width $\Delta' = x/12\Gamma$ (the factor $1/12\Gamma$ is the product of the geometrical factor $1/3$ and the factor $1/4\Gamma$ from the compression of the material by the shock, in accord with the conservation laws of relativistic hydrodynamics).

A necessary condition to accelerate to some energy E'_{max} is that the particle Larmor radius is less than the size scale of the system [22], that is, $r'_L \lesssim x_d/12\Gamma \cdot E_{max}$ in the stationary explosion frame is then given by

$$r'_L = \frac{E'_{max}}{ZeB'} = \frac{E_{max}}{\Gamma ZeB'} < \Delta'. \quad (6)$$

The largest particle energy is reached at the deceleration radius $x = x_d$ when $\Gamma \cong \Gamma_0$, where the

deceleration radius [40]

$$x_d \equiv \left(\frac{3E_0}{4\pi\Gamma_0^2 m_p n_0} \right)^{1/3} \cong 2.6 \times 10^{16} \left(\frac{E_{54}}{\Gamma_{300}^2 n_2} \right)^{1/3} \text{ cm}. \quad (7)$$

Hence $E_{max} \cong ZeB' x_d/12$.

The mean magnetic field B' in the GRB blast wave is assigned in terms of a magnetic field parameter ϵ_B that gives the magnetic field energy density in terms of the energy density of the downstream shocked fluid, so

$$B' = (32\pi n_0 \epsilon_B m_p c^2)^{1/2} \sqrt{\Gamma(\Gamma - 1)} \cong 0.4 \sqrt{\epsilon_B n_0} \Gamma \cong 1200 \sqrt{\epsilon_B n_2} \Gamma_{300} \text{ G}. \quad (8)$$

Thus

$$E_{max} \cong 8 \times 10^{20} Z n_2^{1/6} \epsilon_B^{1/2} \Gamma_{300}^{1/3} E_{54}^{1/3} \text{ eV} \quad (9)$$

[41, 39], so that external shocks of GRBs can accelerate particles to ultra-high and, indeed, super-GZK energies. The highest energies are more easily reached for ions of large Z , which helps to relax limits on density and ϵ_B .

For values appropriate to blazar AGNs, acceleration to UHEs in the external shock of a blazar plasma jet seems possible from eq. 9, at least for FSRQs. For this blazar class, superluminal motion observations [42] and constraints from the requirement that the emission region be optically thin to $\gamma\gamma$ pair production attenuation [43] imply $\Gamma \sim 10 - 30$. The brightest blazar flares observed with EGRET reach $\approx 10^{49} \text{ ergs s}^{-1}$ and last for $\lesssim 1$ day [44], suggesting again that the total isotropic energy release $E_{54} \approx 1$. For $\Gamma \approx 30$, the deceleration time $t_d = (1+z)x_d/\Gamma^2 c$ is shorter than a day, provided that the blazar blast wave passes through a medium of density $\approx 10^2 \text{ cm}^{-3}$. With these numbers, UHECRs can be accelerated in the external shocks of FSRQs. Much improved data for this estimate will be provided with *GLAST*.

The case for UHECR acceleration in BL Lac objects is not as favorable. Although spectral modeling suggests that Γ could be as large as 50 [45], values of Γ inferred from superluminal motion observations rarely exceed 5 – 10 [46]. The mean distances, energy fluxes, and flare durations are generally smaller for BL Lacs than quasars, and

the total energy in BL Lac γ -ray flares is smaller than for FSRQ flares. The deconvolved apparent γ -ray luminosity from PKS 2155-304 flares during the 2006 July flaring state was $\approx 3 \times 10^{45}$ erg s $^{-1}$ [47], and lasts between $\approx 10^2$ and 10^3 s, giving a total apparent energy releases $\approx 3 \times 10^{47} - 3 \times 10^{48}$ ergs. The surrounding medium density is lower in BL Lacs than in FSRQs, given that blazars have smaller optical emission-line equivalent widths than FSRQs, and therefore probably a smaller column density of broad line region material. All these factors make it harder for low- Z ions to reach UHEs. So, if FR I radio galaxies are the sources of UHECRs, then they would have a suppressed proton and low- Z ion content due to acceleration limitations.

Why, however, consider stochastic acceleration processes in the blast waves formed by the external shocks in blazars and GRBs, given that first-order Fermi acceleration through colliding shells, which can operate in both blazars and GRBs, could accelerate the cosmic rays to high energies? The problem here is that the material which forms the outflowing plasma winds is processed through extreme environments around supermassive black holes of blazar AGNs and newly formed black holes in GRBs. Whether ions can survive, as required by the Auger data [5], is an open question. If they do survive, then Wang, Razzaque, & Mészáros [48] have shown that acceleration of UHECR ions to $\gtrsim 10^{20}$ without significant losses to photodisintegration in GRB internal shocks, external shocks, and hypernovae is possible (see also [21]).

In a colliding shell scenario, the ejecta originates from the vicinity of a black hole. For the fireballs that power a GRB, heavier nuclei are broken down into protons and neutrons, deuterium and α particles [49]. Nuclear breakdown reactions, either through direct particle spallation processes or through photodisintegration from the intense radiation field in the vicinity of a black hole, make it questionable if baryonic material ejected from the central engines of black holes in GRBs or blazars has any metal ($A > 4$) content.

In a colliding shell scenario, successive waves of ejecta are supposed to form the flares in blazars and GRBs, and if the hadronic content in the ejecta were composed entirely of protons and light nuclei,

then such an acceleration scenario could not account for the Auger results. Wang, et al. [48] argue, however, that mixing instabilities could develop to seed the relativistic ejecta with heavier ions as the blast wave passes through the the stellar envelope surrounding a GRB. In this case, the amount of baryon contaminant would have to be carefully regulated without heavily loading and quenching the fireballs, unless dirty fireball bursts [50] and quenched, or choked [51] fireballs also occur.

A scenario involving an external shock would permit the capture of ions from the surrounding medium. This medium could be highly enriched from the presence of circumnuclear starbursts surrounding the supermassive black hole in a blazar AGN or OB associations in which a GRB might reside, and so have a considerable ion content. Even if the material had sub-Solar metallicity, heavier ions would be preferentially accelerated due to their larger charge Z (see eq. 9), producing a mixed composition in the UHECRs.

B. Power Requirements for Electrodynamic Acceleration

We apply Waxman's argument [38], giving minimum source power to accelerate $10^{20} E_{20}$ eV protons, to ions. In a region of size R and magnetic field B , electromagnetic forces can accelerate a particle to a maximum energy of $E_{max} > E_{par} \simeq Ze\beta BR$. The available time in the co-moving frame is shortened by bulk Lorentz factor Γ , so that the effective size for acceleration is $\approx R/\Gamma$, and $BR > \Gamma E_{par}/Ze\beta$. The required power of the magnetized flow is

$$L \approx 2 \times 4\pi R^2 v \times \frac{B^2}{8\pi} \approx \beta c (BR)^2 \approx \frac{c\Gamma^2 E_{par}^2}{Z^2 e^2 \beta}$$

or

$$L \cong \frac{3 \times 10^{45}}{Z^2} \frac{\Gamma^2}{\beta} E_{20}^2 \text{ ergs s}^{-1} \\ \cong \frac{5 \times 10^{42}}{(Z/26)^2} \frac{\Gamma^2}{\beta} E_{20}^2 \text{ ergs s}^{-1}, \quad (10)$$

including a factor of 2 for the plasma jet kinetic power. If the nonthermal luminosity is a good measure of jet power, then we can decide whether different source classes are good candidate UHECR sources.

For GRBs, $\Gamma \approx 300$, and $L_{GRB} \gg 10^{50}(\Gamma/300)^2 E_{20}^2/Z^2$ ergs s $^{-1}$. Apparent isotropic X/γ powers of long-duration GRBs are regularly measured in excess of 10^{50} ergs s $^{-1}$ [52], so long-duration GRBs are a viable candidate for UHECR acceleration. For the low-luminosity GRBs, which may only reach $\approx 10^{48} - 10^{50}$ ergs s $^{-1}$ [53], higher Z ions can still be accelerated to super-GZK energies if Γ remains large. It will be interesting to compare radiative powers with this minimum power using allowed values of Γ determined from GLAST data through $\gamma\gamma$ opacity arguments, for different classes of GRBs.

For blazars with $\Gamma \cong 10$, $L_{blazars} \gg 3 \times 10^{47}(\Gamma/10)^2 E_{20}^2/Z^2$ ergs s $^{-1}$. FSRQ blazar γ -ray flares brighter than $\approx 10^{47}$ ergs s $^{-1}$ were frequently detected with EGRET [54]. Present data does not exclude FSRQ blazars from being the sources of UHECRs, especially if the accelerated UHECRs are primarily heavy ions. Comparisons between measured γ -ray luminosity and minimum power requirements using values of Γ obtained from $\gamma\gamma$ arguments, both of which can be determined from GLAST LAT data, can decide whether FSRQ blazars can accelerate UHECR protons and ions.

Eq. (10) shows that it is more difficult to accelerate UHECRs, especially UHECR protons, in the lower luminosity X-ray/TeV blazars with apparent γ -ray powers $\lesssim 10^{45}$ ergs s $^{-1}$. If TeV observations with VERITAS, HESS, or MAGIC were to require, either from spectral modeling or $\gamma\gamma$ arguments, that $\Gamma \gtrsim 50$ in sources like Mrk 421, Mrk 501, or PKS 2155-304, acceleration even of Fe to super-GZK energies might be problematic in the BL Lac sources.

It is also interesting to apply eq. (10) to parameters of merging clusters of galaxies, which have also been studied as a potential source of UHECRs [55, 56].

The gain in kinetic energy when the minor cluster of mass $M_2 = 10^{14} M_{14} M_\odot$, treated as a test particle in the mass distribution of the dominant cluster of mass $M_1 = 10^{15} M_{15} M_\odot$, falls from radius r_1 to radius $r_2 (\leq r_1)$, is $M_2 v_2^2/2 = GM_1 M_2 (r_2^{-1} - r_1^{-1})$ (e.g., [57]). Thus $v \cong \sqrt{2GM_1/r_2}$ when

$r_2 \ll r_1$, and

$$v_2 = \beta_{cl} c \approx 3000 \sqrt{\frac{M_{15}}{r_2(\text{Mpc})}} \text{ km s}^{-1}, \quad (11)$$

so $\beta_{cl} \simeq 10^{-3}$. If r_2 is scaled to a typical core radius of the dominant cluster, ≈ 0.25 Mpc, the greater power output during this merging episode occurs during a timescale shorter by a factor $r^{3/2}$. This can be shown by noting that the characteristic merger time \hat{t} is determined by the acceleration $a = GM_1/r_1^2$ at the outer radius. Because $r_1 \approx a_2 \hat{t}^2/2$,

$$\hat{t} \cong \sqrt{\frac{2r_1^3}{GM_1}} \approx 660 \frac{r_{\text{Mpc}}^{3/2}}{M_{15}} \text{ Myr}, \quad (12)$$

where $r_1 = r_{\text{Mpc}}$ Mpc. The available energy in the collision is

$$\mathcal{E} \approx \frac{GM_1 M_2}{r_1} \approx \frac{8 \times 10^{63}}{r_{\text{Mpc}}} M_{15} M_{14} \text{ ergs}. \quad (13)$$

The ratio of eqs. (13) and (12) gives the maximum power available from the gravitational energy of the merging clusters, namely

$$L_{cl} = \frac{\mathcal{E}}{\hat{t}} \cong 4 \times 10^{47} \frac{M_{15}^2}{r_{\text{Mpc}}^{5/2}} M_{14} \text{ ergs s}^{-1}, \quad (14)$$

When $r_{\text{Mpc}} \sim 0.25$, corresponding to typical core radii of galaxy clusters like Coma, the maximum merger power is ≈ 30 larger and the timescale, eq. (12), is a factor ≈ 8 less. The luminosity requirement to accelerate UHECRs with energy E_{20} is, for parameters typical of merging cluster,

$$L_{gc} \gtrsim 3 \times 10^{48} E_{20}^2 / [Z^2 (\beta_{cl}/10^{-3})] \text{ ergs s}^{-1},$$

from eq. (10). According to this criterion, it is not difficult to accelerate UHECR protons in galaxy cluster environments. This estimate does not consider actual timescales [58] of acceleration, which result in maximum proton energies $\lesssim 10^{19}$ eV for p from nonrelativistic shocks [59]. Acceleration of p to $\lesssim 10^{19}$ eV and Fe to $\lesssim 10^{20}$ eV is possible [56] in large Mach number [60] cluster accretion shocks.

The time for the merger during maximum power output, from eq. (12), corresponds to a distance

$\hat{r} = c\hat{t} \cong 25(r_{\text{Mpc}}/0.25 \text{ Mpc})^{3/2}/M_{15} \text{ Mpc}$, and UHECR Fe might go through some significant photo-erosion in the CMBR and EBL, so Fe would have difficulty surviving to $\gtrsim 10^{20} \text{ eV}$ if it were accelerated by merger shocks in merging clusters of galaxies (cf. [58] for cluster accretion shocks).

X-ray and γ -ray Signatures of UHECR Acceleration

Indirect evidence for UHECR acceleration is given by analysis of spectra and light curves of GRBs and blazars. In the relativistic blastwave framework, the hard X/γ radiation during the prompt phase of a GRB is primarily nonthermal synchrotron radiation, including perhaps some thermal photospheric emission [61]. A synchrotron self-Compton (SSC) component would accompany the nonthermal synchrotron emission, and display a correlated behavior.

The delayed hard emission tail in GRB 940217 [62], lasting for over 90 minutes after the start of the GRB, could be a signature of a long lasting, hadronic acceleration process. The slower decay of the hadronic emission component compared to the leptonic component, as expected from the standard blast wave model [63], might explain the delayed emission. Nevertheless, a leptonic model with an SSC component appearing in the GeV regime when the synchrotron component has decayed to optical/UV energies could also account for the delayed behavior of GRB 940217, or the superbowl burst, GRB 930131 [64].

A more difficult case to explain in terms of non-thermal lepton radiations is GRB 941017, observed with the BATSE Large Area Detector (LAD) and the EGRET Total Absorption Shower Counter (TASC). González et al. [65] reported the detection of an anomalous MeV emission component in the spectrum of this burst that decays more slowly than the prompt emission detected with the LAD between $\approx 50 \text{ keV}$ and 1 MeV range. The multi-MeV component lasts for $\gtrsim 200$ seconds, and is detected both with the BATSE LAD near 1 MeV and with the EGRET TASC between ≈ 1 and 200 MeV . The spectrum is very hard, with a photon number flux $\phi(\epsilon_\gamma) \propto \epsilon_\gamma^{-1}$, where ϵ_γ is the observed photon energy.

This component was not predicted nor is easily explained within the standard leptonic model for GRB blast waves. It has been suggested that this emission component could be related to Comptonization of reverse-shock photons by the forward shock electrons, including self-absorbed reverse-shock optical synchrotron radiation [66]. Extremely large apparent isotropic energies are however required.

This component could be a consequence of the acceleration of ultrarelativistic hadrons at the relativistic shocks of GRBs [67]. A pair-photon cascade initiated by photohadronic processes between high-energy hadrons accelerated in the GRB blast wave and the internal synchrotron radiation field produces an emission component that appears during the prompt phase, as shown in Fig. 3, but delayed due to the time required for acceleration. Photomeson interactions in the relativistic blast wave would simultaneously make a beam of UHE neutrons and neutrinos, as proposed for blazar jets [68]. Subsequent photopion production of these neutrons with photons outside the blast wave will produce a directed hyperrelativistic electron-positron beam in the process of charged pion decay and the conversion of high-energy photons formed in π^0 decay. These energetic leptons produce a synchrotron spectrum in the radiation reaction-limited regime extending to $\gtrsim \text{GeV}$ energies, with properties in the $1 - 200 \text{ MeV}$ range similar to that measured from GRB 941017. GRBs displaying anomalous γ -ray components are most likely to be detected as sources of high-energy neutrinos with IceCube.

If UHECRs are accelerated by GRB blast waves, then blast-wave dynamics will be affected by the loss of internal energy when the UHECRs escape. This effect [69] could explain the rapid X-ray declines in the Swift GRB light curves [70]. Protons undergoing photopion interactions with photons at the peak photon frequency ν_{pk} or peak dimensionless energy $\epsilon_{pk} = h\nu_{pk}/m_e c^2 \cong 2\Gamma\epsilon'_{pk}/(1+z)$ of the νF_ν spectrum have energy, as measured by an observer in the explosion frame,

$$E_{pk} = m_p c^2 \gamma_{pk} \simeq \frac{3 \times 10^{16} (\Gamma/300)^2}{(1+z)\epsilon_{pk}} \text{ eV}. \quad (15)$$

The comoving time required for a proton with energy E_{pk} to lose a significant fraction of its energy

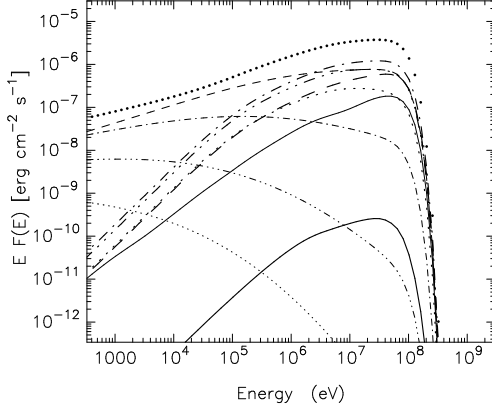


Figure 3: Atoyan’s calculation of photon energy flux from an electromagnetic cascade initiated by photopion secondaries in a model GRB, with parameters given in Ref. [67]. Five generations of Compton (heavy curves) and synchrotron (light curves) are shown. The first through fifth generations are given by solid, dashed, dot-dashed, dot-triple-dashed, and dotted curves, respectively. The total cascade radiation spectrum is given by the upper bold dotted curve.

through photohadronic processes is

$$t'_{\phi\pi}(E_{pk}) \simeq \frac{m_e c^2 x^2 \Gamma^2 \epsilon'_{pk}}{K_{\phi\pi} \sigma_{\phi\pi} d_L^2 f_{\epsilon_{pk}}} \simeq 2 \times 10^6 \frac{x_{16}^2 (\Gamma/300)(1+z)\epsilon_{pk}}{d_{28}^2 f_{-6}} \text{ s}, \quad (16)$$

where $x = 10^{16} x_{16}$ cm and $f_{\epsilon_{pk}} = 10^{-6} f_{-6}$ ergs cm $^{-2}$ s $^{-1}$ is the νF_ν flux measured at ϵ_{pk} ; the relation between E_{pk} and ϵ_{pk} is given by eq. (15).

The dependence of the terms $x(t)$, $f_{\epsilon_{pk}}(t)$, $\Gamma(t)$, and $\epsilon_{pk}(t)$ on observer time in eq. (16) can be analytically expressed for the external shock model in terms of the GRB blast wave properties E_0 , Γ_0 , environmental parameters, e.g., n_0 , and microphysical blast wave parameters ϵ_B and ϵ_e [69]. This can also be done for other important timescales, for example, the (available) comoving time t'_{ava} since the start of the GRB explosion, the comoving acceleration time $t'_{acc} = \zeta_{acc} m_p c^2 \gamma' / e B c$, written as a factor $\zeta_{acc} \gg 1$ times the Larmor timescale [71] ($\zeta_{acc} = 10$ in the Figure 3), the escape timescale t'_{esc} in the Bohm diffusion approx-

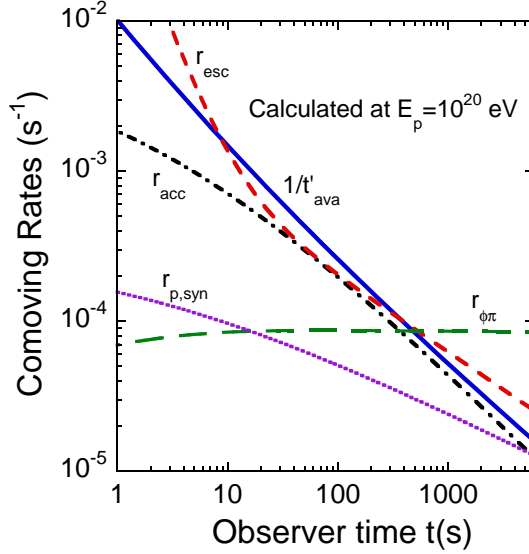


Figure 4: Rates and inverse timescales as a function of observer time for 10^{20} eV cosmic ray protons as measured by a stationary external observer. The figure uses parameters given in the text.

imation, and the proton synchrotron energy loss timescale t'_{syn} .

Fig. 4 shows the rates (or the inverse of the timescales) for 10^{20} eV protons in the case of an adiabatic blast wave that decelerates in a uniform surrounding medium. The parameters are

$$z = 1, \Gamma_0 = 150, E_{54} = 10, n_0 = 1000 \text{ cm}^{-3}, \\ \epsilon_e = 0.1, \text{ and } \epsilon_B = 0.3.$$

For these parameters, it takes a few hundred seconds to accelerate protons to energies $\approx 10^{20}$ eV, at which time photohadronic losses and escape start to be important. Photohadronic losses inject electrons and photons into the GRB blast wave. The electromagnetic cascade emission, in addition to hyperrelativistic electron synchrotron radiation from neutron escape followed by subsequent photohadronic interactions [67], makes a delayed anomalous γ -ray emission component as observed in GRBs 940217 and 941017 [62, 65]. Ultra-high energy neutrino secondaries are produced as by-products of the hadronically-induced cascade. The ultra-high energy neutrons and escaping protons, accompanied by escaping UHECR ions, form the

UHECRs with energies $\gtrsim 10^{20}$ eV. Detection of high-energy neutrinos from GRBs would confirm the importance of hadronic processes in GRB blast waves.

The GRB blast wave quickly loses internal energy due to the photohadronic processes and particle escape. The blast wave will then decelerate, producing a rapidly decaying X-ray flux. I [69] argue that the decaying fluxes in Swift GRBs are signatures of UHECR acceleration by GRBs. (See [72] for other explanations of the Swift data.) If this scenario is correct, GLAST will detect anomalous γ -ray components preferentially in those GRBs that undergo rapid X-ray declines in their X-ray light curves.

Anomalous γ -ray signatures have also been detected in the spectra of blazar AGNs, for example, the orphan γ -ray flare observed in the TeV blazar 1ES 1959+650 [73]. This is a case where the correlated variability between the synchrotron X-rays and SSC γ rays expected in the standard synchrotron/SSC TeV blazar model is not observed. Orphan X-ray flares from an hadronic emission component could be produced by cosmic ray protons with Lorentz factors $\gamma \approx 10^2 - 10^4$ undergoing photohadronic interactions with reflected X-ray target photons [74]. The implied neutrino signature is unfortunately too weak to be detected with IceCube [75] or a Northern Hemisphere km-scale neutrino telescope. In order for a TeV blazar to have efficient photohadronic interactions of UHECR protons with ambient jet synchrotron radiation, the blazar must be optically thick to $\gamma\gamma$ pair production [76, 77], so we would only expect PeV neutrinos from TeV blazars during times of low-state TeV γ ray flux. Important for this search is multiwavelength GRB and blazar capability.

In the case of FSRQ blazars, there is as yet no strong evidence for anomalous γ -ray emission components that could be associated with UHECR acceleration. This lack of evidence should not be considered definitive, for a number of reasons: (1) The leptonic models for FSRQs are more complicated than for TeV blazars or GRBs, and involve a variety of external radiation fields and, consequently, more parameters. Back-scattered radiation in structured blazar AGN environments makes another radiation feature. This makes it more difficult to ascribe an emission component to a non-

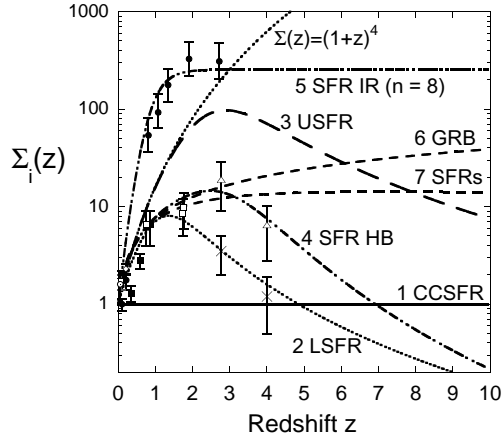


Figure 5: Different star formation rate (SFR) histories, as described in the text.

leptonic origin. (2) Except in a few cases, e.g., [78, 79], the γ -ray data from FSRQs taken during the EGRET era didn't have extensive multi-wavelength monitoring. (3) The sensitivity of the EGRET telescope permitted spectral fits with a single power law integrated over several days in all but a few cases. This situation will change dramatically with the launch of GLAST in 2008, and is already changing with the development of low-energy threshold air-Cherenkov γ -ray detectors. A significant advance in this direction was reported at this conference by the MAGIC collaboration [80], namely the 6 and 5 σ detections of 3C 279 ($z \cong 0.538$) in the respective bands $\sim 80 - 220$ GeV and $\gtrsim 220$ GeV. This opens the question of what other nearby FSRQs will be detected with MAGIC, and what this means for the intensity of the EBL.

UHECR Protons from GRBs

GRBs are argued to be the sources of the UHECRs for over a decade [24, 25, 81]. Well-defined calculations based on particle physics and GRB astronomy for UHECR proton propagation in the expanding universe, treating expansion, and photopion and photopair interactions with CMBR photons only (see Figure 1), give results that can be compared with data and used to benchmark more

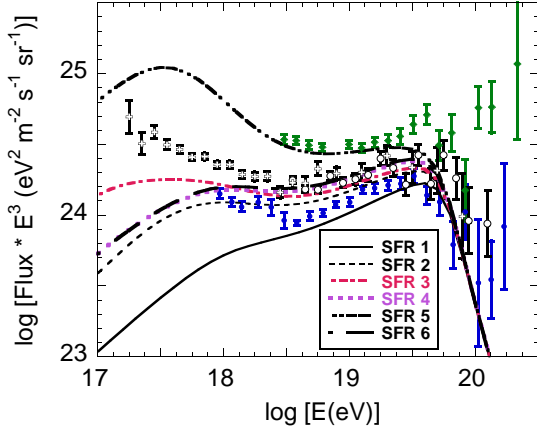


Figure 6: UHECR data from monocular HiRes (open crosses and circles), Auger (filled circles), and AGASA (filled diamonds) data, compared with GRB predictions for UHECR protons with different SFRs shown in Fig. 5. Protons are injected from 10^{14} eV to an exponential cutoff energy $E_{max} = 10^{20}$ eV with local emissivity $= 60 \times 10^{44}$ ergs Mpc $^{-3}$ yr $^{-1}$.

detailed calculations involving nuclei and various source classes.

Restricted to the long-duration class, of which we have the most knowledge, the act of making a calculation of the UHECR spectrum from GRBs requires (i) an injection spectrum, which we take to be a power-law with number injection index $s = 2.2$ between 10^{14} eV and an exponential cutoff energy, usually taken to be 10^{20} eV; (ii) a local emissivity, which acts as an overall normalization factor on the UHECR spectrum; and (iii) a star formation rate (SFR). Here the underlying assumption is that the rate-density of GRBs follows star formation activity, expressed in terms of the mass processed into stars per comoving volume, and assumed to be traced primarily by hot young stars. Knowledge of the SFR is obtained by analyzing the blue/UV luminosity density using statistical samples of galaxies. Blue light is thought to be a good proxy of star-formation activity, but extinction by dust complicates the measurement.

Fig. 5 shows various SFRs based on different approaches to the problem. SFR 4, from Hopkins and Beacom [82], is based on a compilation of IR, optical, and UV data. SFR 1 gives the lowest accept-

able rate compatible with the data. SFR 3 gives the rate assuming large extinction corrections, and was used to fit the UHECR spectrum in [31]. With this rapidly increasing rate density of GRBs at redshifts $z \approx 1 - 3$, a large pair production trough at $\approx 10^{18.4}$ eV is formed [83]. A rate density of GRBs following the extremely active SFR 5, based on IR luminosity density, is ruled out from calculations of the UHECR spectrum, as can be seen in Fig. 6.

A statistical study [84] of the redshift and opening-angle distribution of GRBs observed before Swift, primarily Beppo-SAX GRBs, and the z -distribution of GRBs observed with Swift, rejects SFR 3 for GRBs based on a standard relativistic jet model. We concluded that the GRB rate density must monotonically increase to $z \approx 5 - 7$ to explain the GRB statistics. The UHECR spectrum from SFR 6, seen in Fig. 6, gives a reasonable fit to the HiRes data (the SFR 7 spectrum is nearly the same). Normalization to the Auger data would change the emissivity normalization down by a factor $\approx 1/3$.

The idealized $SFR \propto (1 + z)^4$ sketched in Fig. 5 was used by Berezhinsky and his collaborators [85, 86] to describe the SFR activity of the UHECR sources, possibly blazars. Such extreme SFR activity produces a large pair production trough, and they proposed that the ankle/dip feature in the UHECR spectrum is due to photopair losses. Reasonable fits to the HiRes data were obtained with injection indices into intergalactic space $s \approx 2.7$.

This model $SFR \propto (1 + z)^4$ can hardly be correct, but models of blazars are more difficult than of GRBs by requiring both luminosity and density evolution. The long-duration GRB engine could very well be unchanged with epoch, but both due to black hole growth and fueling, the UHECR output from blazars must change with time. This behavior is not well understood, so a mathematical model might be the best that can be done pending better studies (cf. [34]).

Figure 7 shows predictions of the total diffuse neutrino intensity spectrum for the various GRB models in Figure 6, compared with the ANITA sensitivity for a 45 day flight [87], and an estimated sensitivity for the proposed ARIANNA project [88]. Long-duration balloon-borne high-energy neutrino telescopes can already start to test SFR 3 used in

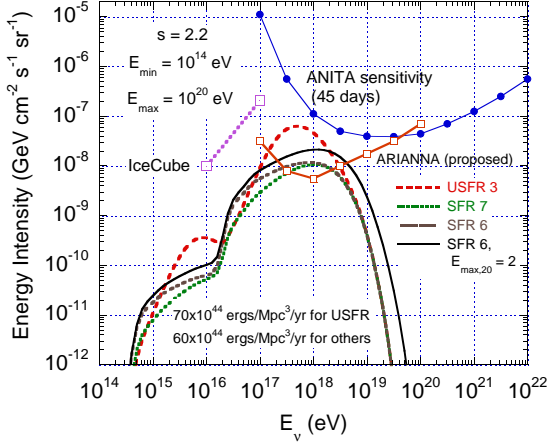


Figure 7: Comparison of model calculations of GZK neutrino intensities for neutrinos of all flavors with sensitivity curves as labeled.

our GRB model for UHECRs [31], and is close to discovering the guaranteed flux of GZK neutrinos. The cosmogenic neutrino flux from GRBs is difficult to detect with IceCube, which is more sensitive to cosmic PeV sources (see [89] for IceCube sensitivities).

Survival of UHECR Ions in the Blazar Environment

Spurred by the Auger results on composition [5], we examine whether UHECRs can leave the blazar environment without being significantly photo-eroded. This assumes that blazar jets accelerate UHECRs, which is feasible given that the UHECR spectrum can be fit using simple assumptions for the SFR activity and injection spectrum [85, 86]. γ rays from blazars could be a consequence of ultra-relativistic hadrons in blazar jets [90, 68]. Cosmic rays accelerated in the inner blazar jet can power the knots and lobes of FR II radio galaxies through UHE beamed neutral production and escape due to photopion interactions of UHECR protons with ambient radiation in the inner jet [68]. The formation of a neutral beam in FR II radio galaxies could explain the Chandra X-ray emission from knots and hot spots in radio galaxies [91] by a second synchrotron component induced by UHECR activity [92].

Crucial to efficient neutrino and neutral beam power is that the blazar jet is found within the BLR where the scattered radiation field is intense. The question of the location of the γ -ray production site [93, 94], which would almost certainly be the location of the UHECR accelerator, will be settled by correlated GLAST/radio observations.

Ions accelerated in the inner jets of BL Lac objects and FR I radio galaxies can pass through the broad line region (BLR) without significant photodisintegration, as we now show. Underlying this estimate is the unification scenario for blazars as expressed in [95], in which FR Is are the parent population of BL Lac objects, and FR IIs are the parent population of FSRQs.

Let the blazar BLR be approximated by a spherically-symmetric distribution of scattering electrons with density $n_0(x)$ at distance x from the central source. The scattered radiation density in blazars can be estimated by noting that a fraction $\approx n_0(x)\sigma_T(x/2)$ of the ambient photons will be scattered within a shell of width $\approx x/2$. For an isotropically emitting central source of radiation with photon production rate $\dot{N}_{ph}(\epsilon)$ per unit dimensionless photon energy $\epsilon = h\nu/m_e c^2$, the ambient photon density from the central source emission is $n_{ph}(\epsilon; x) = \dot{N}_{ph}(\epsilon)/4\pi x^2 c$. For assumed isotropic Thomson scattering, the spectral density of scattered radiation is

$$n_{sc}(\epsilon; x) \approx \frac{n_0(x)\sigma_T\dot{N}_{ph}(\epsilon)}{8\pi x c} \quad (17)$$

[96, 97, 98].

The central source emission is assumed to be radiated by an accretion disk around the supermassive black hole. We represent the blue-bump emission, commonly observed in Seyfert galaxies (it is difficult to observe in blazars because of the luminous jet radiation), by a Shakura-Sunyaev disk spectrum of the form

$$\dot{N}_{ph}(\epsilon) = L_0 \frac{\epsilon^{-2/3} \exp(-\epsilon/\epsilon_{max})}{m_e c^2 \epsilon_{max}^{4/3} \Gamma(4/3)}, \quad (18)$$

normalized to the total Shakura-Sunyaev disk luminosity $L_0 = 10^{46} L_{46} \text{ ergs s}^{-1}$, where $\Gamma(4/3) \cong 0.893$, and ϵ_{max} is the maximum photon energy radiated in the disk spectrum. For the UV bump observed in supermassive black holes, $\epsilon_{-5} \equiv \epsilon_{max}/10^{-5} \cong 1$.

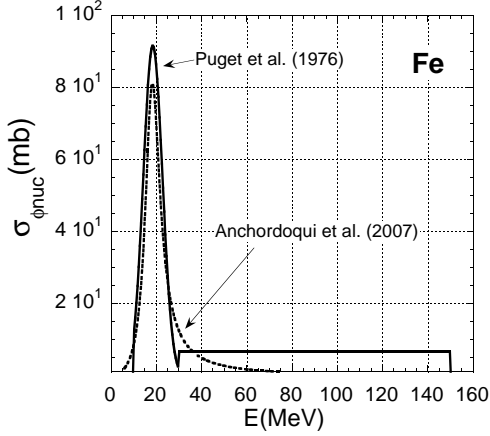


Figure 8: Comparison of photo-nuclear destruction cross section for Fe from [12] and [101].

The blue bump in 3C 273 reaches a νF_ν peak flux of $\approx 3 \times 10^{-10}$ ergs cm $^{-2}$ s $^{-1}$ at ≈ 10 eV, corresponding to $\nu L_\nu \approx 2 \times 10^{46}$ ergs s $^{-1}$ and $\epsilon_{-5} \approx 2$ [99]. The hard UV emission component observed from 3C 279 with IUE [100] has a peak νL_ν luminosity $\approx 3 \times 10^{45}$ ergs s $^{-1}$. Its effective temperature is $\approx 20,000$ K, corresponding to a mean dimensionless photon energy $\approx 10^{-5}$.

A δ -function approximation for the photodisintegration cross section of a nucleus with atomic mass $A = 56A_{56}$ is

$$\sigma_A(\epsilon_r) \cong \frac{\pi}{2} \sigma_{0,A} \Delta \delta(\epsilon_r - \epsilon_{r,0}), \quad (19)$$

[101], where $\sigma_{0,A} = 1.45A$ mb, $\Delta \cong 15.6$, $\epsilon_{r,0} \cong 83.5A^{0.21}$, and ϵ_r is the invariant dimensionless photon energy in the ion's rest frame. A comparison of the photonuclear destruction cross sections for Fe is shown in Fig. 8. The δ -function approximation should be fairly good in all cases where the target photon spectrum is not too hard.

For an ultra-relativistic ion passing through an isotropic radiation field, the probability per unit pathlength for the ion to photodisintegrate by interacting with ambient photons is given by

$$\frac{dN_{\phi nuc}}{dx} = (2\gamma^2)^{-1} \times \int_0^\infty d\epsilon \epsilon^{-2} n_{ph}(\epsilon) \int_0^{2\gamma\epsilon} d\epsilon_r \epsilon_r \sigma_A(\epsilon_r), \quad (20)$$

where the particle Lorentz factor $\gamma = E/Am_p c^2$.

The probability of an UHECR ion photo-disintegrating as it travels through the AGN BLR is, using eqs. (17) – (19) in eq. (20), simply

$$P_{\phi nuc} \cong x \frac{dN_{\phi nuc}}{dx} \approx \frac{\sigma_{0,A} \Delta \epsilon_{r,0} n_0(x) \sigma_T L_0}{32\Gamma(4/3) \gamma^2 m_e^3 \epsilon_{max}^3} \int_{u_0}^\infty du u^{-8/3} \exp(-u), \quad (21)$$

where $u_0 \equiv \epsilon_{r,0}/2\gamma\epsilon_{max}$.

Here we take the typical extent of the BLR as $\approx 0.1 - 1$ pc, and mean optical depth $\tau_T \lesssim 0.1$. The BLR medium is probably clumped in rather dense clouds and has a strong density gradient from the BLR to the narrow line region [102, 103], but here we approximate it as being rather uniform within a shell of radius $10^{18} R_{18}$ cm with Thomson depth $\tau_T = 10^{-2} \tau_{-2}$, so that the mean BLR density is $n_0 \cong 1.5 \times 10^4 \tau_{-2}/R_{18}$ cm $^{-3}$.

Eq. (21) is easily solved in the limit $u_0 \ll 1$ or

$$E \gg \frac{4 \times 10^{15}}{\epsilon_{-5}} A^{0.79} \text{ eV}.$$

The result is

$$P_{\phi nuc} \cong 0.12 \frac{A_{56}^{1.47} L_{46} \tau_{-2}}{E_{20}^{1/3} \epsilon_{-5}^{4/3} R_{18}}, \quad (22)$$

for $E_{20} \gg 10^{-3} A_{56}^{0.79}/\epsilon_{-5}$.

This result indicates that for typical parameters that may characterize the BLR of BL Lac objects, with $\tau_{-2} \lesssim 1$ and $L_0 \approx 10^{44}$ ergs s $^{-1}$, UHECR ions will escape without undergoing photonuclear breakup. The BLR environment may pose a hazard to UHECR ion escape in the luminous FR II radio galaxies and FSRQs with broad optical emission lines. But note that our calculation only considered a single interaction with the loss of one or a few nucleons from the UHECR ion. The corresponding probability for complete breakup will be a factor $\approx A/2$ smaller.

This estimate suggests that UHECR ions can escape from BL Lacs and also from FSRQs, except in the cases of the most luminous blazars with thick columns of BLR material. The scattered radiation field in blazars is a convolution of the central source luminosity and surrounding gas distribution. The $\gamma\gamma$ attenuation process gives a separate probe of this radiation field [96, 104, 105]. By

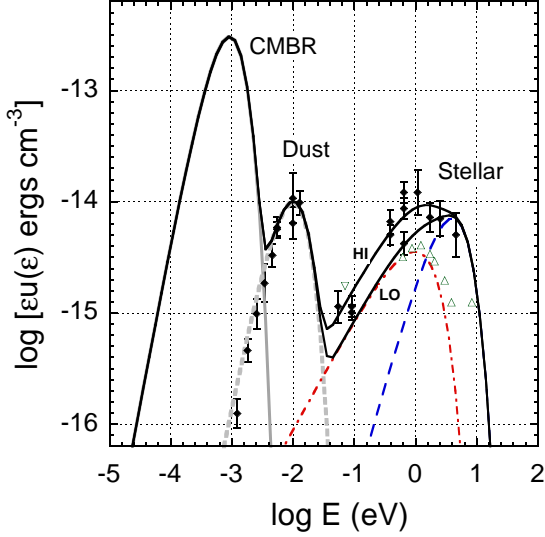


Figure 9: Measurements of the EBL at optical and infrared frequencies [106], plotted in terms of spectral energy density $\epsilon u(\epsilon)$, and fits to the EBL using modified blackbody functions. Data triangles pointed upwards refer to lower limits, and data triangles pointed downwards refer to upper limits. The spectral energy density of the CMBR at $z = 0$ is also shown.

jointly analyzing photodisintegration and $\gamma\gamma$ processes, GLAST data can be used to determine if the black hole jet environment limits UHECR escape.

The Extragalactic Background Light

Fig. 9 shows measurements of the intensity of the unresolved IR and optical EBL at the present epoch from the review by Hauser and Dwek [106, 107], including an upper limit at ≈ 0.1 eV inferred from γ -ray observations [108]. Motivated by the appearance of two distinct peaks in the SED of luminous infrared galaxies [109, 110], by synoptic spectra of galaxies in the Sloan Digital Sky Survey [111], by SEDs of nearby normal galaxies, including data from the *Spitzer Space Telescope* [112] and normal star-forming galaxies like the Milky Way [113], I fit these two peaks with modified blackbody functions. The lower energy emission feature peaking near ≈ 0.01 eV, probably due to radiation repro-

Table 2: Properties of the Dust and Two Stellar Components

Component	$T(K)$	u_0 (10^{-14} ergs cm^{-3})	k
Dust	31	0.273	3.8
Star 1 (HI EBL)	7100	1.1	2.0
Star 1 (LO EBL)	7100	$1.1 \div 2$	2.0
Star 2	16,600	0.5	3.0

cessed by dust, is referred to as the dust component. The higher energy emission feature peaking near 2 eV is referred to as the stellar component. In our calculations, two modified blackbodies make up the stellar component. More terms can be added as required.

The modified blackbody spectral energy density is written in the form

$$\epsilon u(\epsilon) = u_0 \frac{w^k}{\exp(w) - 1} = m_e c^2 \epsilon^2 n_{ph}(\epsilon), \quad (23)$$

where $w \equiv \epsilon/\Theta$. For a blackbody, $k = 4$ and $u_0 = 8\pi m_e c^2 \Theta_0^4 (1+z)^4 / \lambda_C^3 = 6.37 \times 10^{-14} (1+z)^4$ ergs cm^{-3} . The fits to the data in Fig. 9 use the parameters given in Table 2. The high and low EBLs differ only by a factor 2 for the intensity of the lower temperature stellar radiation field.

Fig. 10 shows the optical depth to $\gamma\gamma$ pair production attenuation for γ rays with measured energies E detected from the TeV XBL 1ES 1101-232 at $z = 0.186$ [114, 115]. Separate components for the CMBR, dust, and stellar radiation fields are shown for the low EBL in the figure. In making this calculation, only the CMBR field evolves with redshift, and the dust and stellar radiation field energy densities remain roughly constant. This assumption becomes increasingly less reliable at higher redshifts.

The attenuation factor, from which the intrinsic spectrum of 1ES 1101-232 is obtained, is plotted in Fig. 11. As can be seen from the index, the use of the low EBL means that the intrinsic photon spectral index of 1ES 1101-232 from $\approx 0.2 - 3$ TeV is ≈ -2.0 . If we adopt as a general rule, consistent with our knowledge of the GeV spectra of FSRQs [44] and GeV – TeV spectra of BL

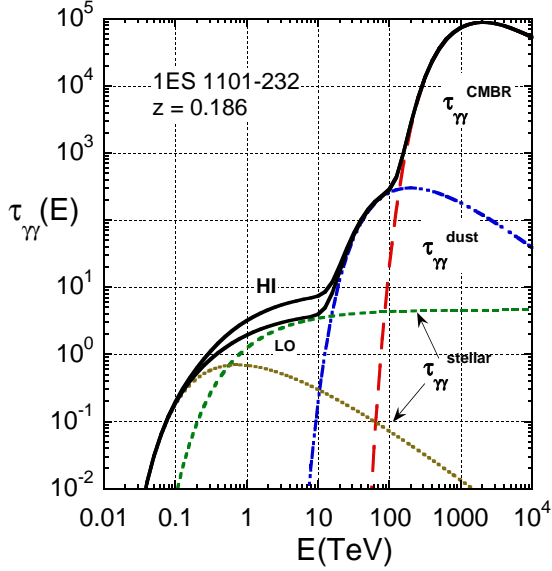


Figure 10: Optical depth for a source at $z = 0.186$ to $\gamma\gamma$ attenuation for the low and high forms for the EBL shown in Fig. 9.

Lacs like Mrk 421 and Mrk 501, that the intrinsic spectrum is softer than -2 , then the low EBL is favored (cf. [116, 117]). A low EBL between 1 and 10 μ solves the problem of the unusually hard γ -ray spectrum of 1ES 1101-232 [118, 114], and avoids having to construct acceleration scenarios not operating in Mrk 421 and Mrk 501, and to explain lack of evidence of hard synchrotron components associated with a hard electron component in TeV/XBLs.

The low EBL with a steep 2 – 10 micron spectrum favored to explain the TeV blazar data is in general agreement with the Primack model for galaxy formation [119], which considers star formation, supernova feedback and metal production in merging dark matter halos. The low EBL disagrees with the EBL derived by Stecker and collaborators [120, 121, 122]. The problem is that their empirical data base relies heavily on IRAS data at 12, 25, 60, and 100 μ and uses a poor representation of the galactic SEDs between 1 and 10 μ . Individual IR and normal galaxies show far more structure in this region than considered.

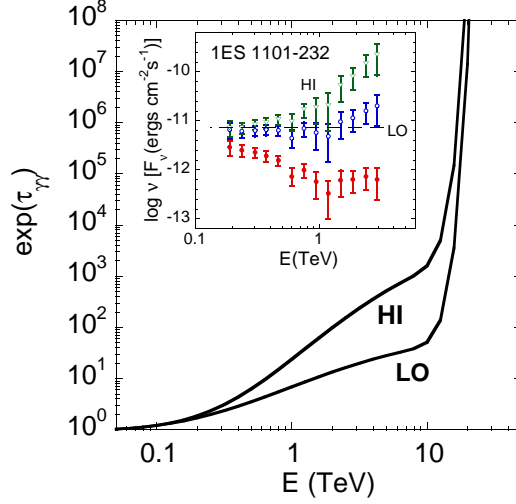


Figure 11: Attenuation factor for the low and high forms of the EBL, for 1ES 1101-232 at $z = 0.186$. Inset shows the effects of the low and high EBLs on the intrinsic spectrum of 1ES 1101-232 [118, 114].

The γ -Ray Horizon

The low and high EBL SEDs represent the likely range of the local $z \ll 1$ IGM IR and optical radiation fields. We can use this field to calculate the photon horizon where $\tau_{\gamma\gamma}(E, z) = 1$ [123, 124] in the limit $z \ll 1$, when the IR and optical radiation fields have not changed appreciably over time. The result is shown in Fig. 12. This diagram is primarily illustrative, and in some respects misleading. At the redshift of 1ES 1101-232, namely $z = 0.186$, this diagram says that the exponential cutoff energy is at $\approx 300 - 400$ GeV, and that the low and high EBLs are not significantly different. In fact, no exponential cutoff is seen in the 1ES 1101-232 TeV spectrum (see inset to Figure 11), because the actual attenuation is very sensitive to the full spectrum of the EBL.

This figure does illustrate that PeV γ -rays can be detected from sources within our Galaxy, though they might be subject to modest attenuation from the CMBR. The IR and stellar radiation fields can also contribute significant $\gamma\gamma$ opacity at ~ 100 TeV. Anisotropy effects of the radiation fields on opacity have recently been calculated by [113, 125]. Attenuated spectra of TeV – PeV γ -ray

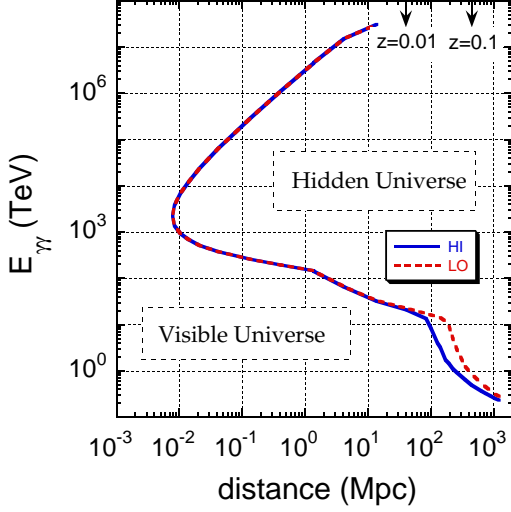


Figure 12: Low redshift ($z \ll 1$) γ -ray horizon giving the relationship between photon energy and z or distance where $\tau_{\gamma\gamma}(E, z) = 1$ for the low and high EBLs shown in Fig. 11. Calculated up to $z = 0.25$.

sources could in principle give a distance measure of specific sources in the Milky Way and nearby galaxies.

The UHECR Ion GZK Radius

We now use our low and high estimates of the EBL to calculate the ion GZK radius. First we show, in Figure 13, the energy loss and interaction mean-free paths for UHECR protons interacting with the combined EBL and CMBR, with components as shown. The dust component makes a minor, $\simeq 10\%$ contribution at $\approx 8 \times 10^{19}$ eV, but could be somewhat larger for a modified fit to the FIR EBL. Other than that, the energy-loss mean free path is essentially given by the CMBR result (Figure 1). Note also that the ratio of the CMBR energy loss and scattering mean-free paths is ≈ 5 on the low-energy wing where protons interact with the exponential Wien portion of the blackbody distribution. This ratio, arising from the 20% inelasticity for direct and resonance pion production, decreases at $\gtrsim 4 \times 10^{20}$ eV due to the greater fraction of multipion interactions at higher energies.

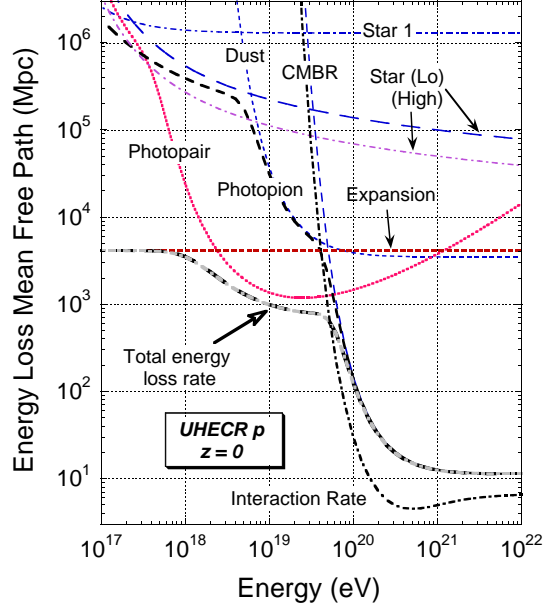


Figure 13: Energy loss mean-free paths for protons in the combined EBL and CMBR radiation fields, including photopion, photopair, and expansion losses. The different low and high EBLs make little difference on the UHECR proton spectrum.

Before calculating ion mean-free paths, it is worth mentioning how the energy-loss formula for photodisintegration is calculated. When a single nucleon is ejected, then an energy loss $\propto 1/A$ of the original energy E happens (technically, provided that the nucleon ejection is isotropic in the nucleon frame), and for the ejection of two nucleons, an energy loss $= 2E/A$ occurs. For multi-nucleon injection, an average factor is used, given by Puget et al. (1976) [12], $= 3.6/A$ for $10 \leq A \leq 22$, and $= 4.349E/A$ for $23 \leq A \leq 56$. A low-energy threshold of 10 MeV is used [13]. Obviously, after a single interaction, the original nucleonic identification is changed, so that new sets of loss rates have to be used for the daughter particles. The calculated MFPs have only a generalized meaning, but provide inputs for accurate Monte Carlo simulations.

Figure 14 gives various contributions of the CMBR and low and high EBLs to the effective energy-loss rate of UHECR Fe in an IGM radiation field at the present epoch. Also shown is the photodis-

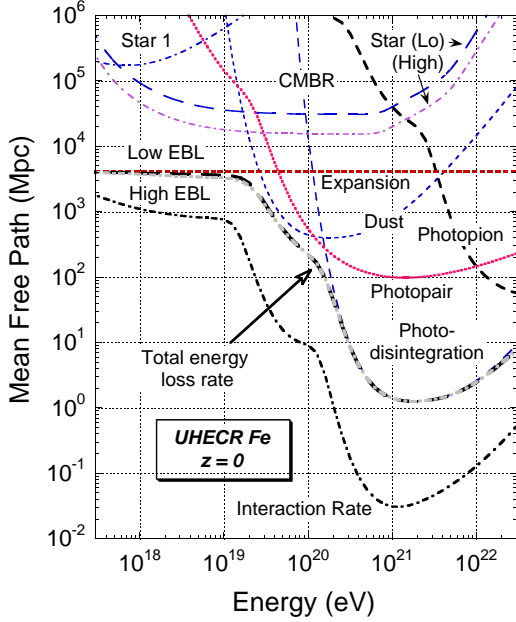


Figure 14: Photonuclear MFPs for UHECR Fe, including separate contributions to photodisintegration, and total energy-loss and interaction rates.

tegration interaction rate for the ejection of at least one nucleon. In effect, the energy-loss MFP gives the distance an Fe ion would have to travel to be broken up into mostly protons and neutrons. For $E \gtrsim 6 \times 10^{19}$ eV, Fe only has to travel $\mathcal{O}(\text{Mpc})$ before being transformed to lighter elements, and could hardly be seen in abundance in the UHECRs above this energy unless UHECR sources reside in the neighborhood of our Galaxy, including M31 and our satellite galaxies (possible for a GRB origin of the UHECRs). Secondary nucleons with $A \sim 56/2$ would be more prevalent due to Fe photo-erosion.

Figure 15 compares different assumptions for the photopion energy-loss rate on the total energy-loss rate of UHECR O in the CMBR and the low EBL. Without a detailed physical model, the photopion cross section should go $\propto A^{2/3}$ for a quasi-spherical nucleon, with a photopion energy-loss rate $\propto A^{2/3}$, giving the maximum MFP. More realistically, only one pion is produced with near threshold energy in the interaction, so the inelasticity would be $\propto A^{-1}$, and the photopion energy-loss rate $\propto A^{-1/3}$, giving the minimum MFP. In

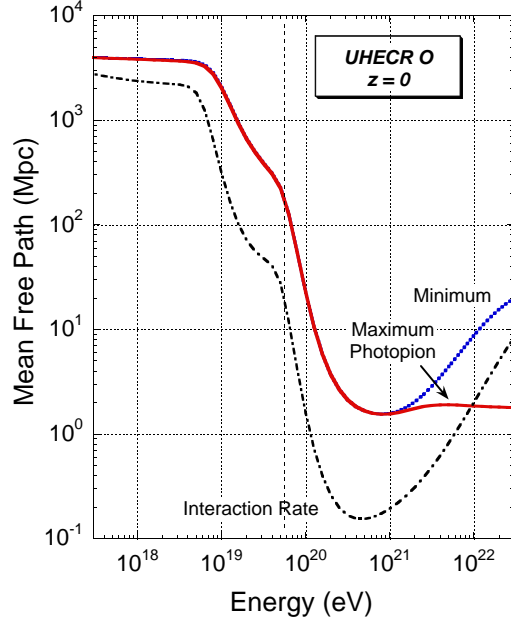


Figure 15: Comparison of the effects on the total energy-loss MFP of UHECR O in the CMBR and low EBL field for different assumptions of the inelasticity in inelastic photopion production.

multi-pion production, the inelasticity should be larger than the minimum, so the “true” photopion energy loss rate should reside between these two extremes. The difference in either case is not significant below 10^{21} eV, as can be seen.

Proton and ion MFPs for energy loss in the combined CMBR and low EBL are shown in Figure 16. Most dramatic is the rapid decrease of the MFP between 10^{19} and 10^{20} eV, precisely where the HiRes and Auger Observatories discover the spectral softening in the UHECR energy spectrum [1, 2]. Keeping in mind that the essential destruction of a nucleus of a given type is proportional to the scattering rate, and that the complete breakup proportional to the energy-loss rate, then this figure shows that structure within 100s of Mpc become visible above $\approx 6 \times 10^{19}$ eV. At these energies, all ions will have undergone significant breakup, so that an original enhancement of Fe would be broken up to smaller Z . With increased statistics, higher energy events should be identified with even closer structures.

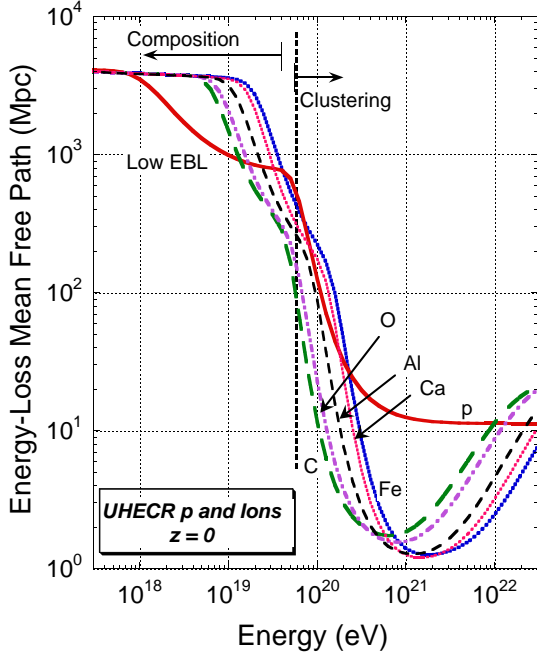


Figure 16: Comparison of energy-loss MFPs of UHECR protons and ions in the combined low EBL and CMBR.

Figure 16 reveals a number of interesting things. First, whereas UHECR protons have significant photopair losses to $\approx 10^{18}$ eV, there is no change in ionic composition below $\approx 5 \times 10^{18}$ eV. At these energies, all ion losses are due to expansion. Above $\approx 5 \times 10^{18}$ eV, corresponding to the ankle or dip energy, photopair and photodestruction losses become roughly equally important. The dust component of the EBL (whose SED is not that accurately known) is important for the rapidly increasing energy-loss rate between $\approx 5 \times 10^{18} - 6 \times 10^{19}$ eV. Above $\approx 6 \times 10^{19}$ eV, photodisintegration by the CMBR starts to dominate, reducing the interaction length to tens of Mpc or less. UHECR Fe injected at $\gtrsim 10^{20}$ eV will, in short order, degrade to lighter nuclei at lower energies, which have larger cross sections at a given energy to degrade the nuclei.

By the accumulation of lighter Z material below the GZK energy, an ankle and cutoff may be formed through the injection of UHECR ions with large $Z \sim 30 - 56$. The formation of this dip, seen in AGASA, HiRes and Auger data, must be ex-

plained in any viable model for UHECRs. The apparently natural explanation of the ankle as a pair production trough resulting from UHECR proton injection [83, 31, 86, 85] might also find an explanation in GZK nucleonic physics. Detailed study requires a Monte Carlo simulation.

IGM Magnetic Field

We use the Auger results [15] to set lower limits on the mean IGM magnetic field B . The equation for the deflection angle from a source at distance d is [25, 126]

$$\theta_d \simeq \frac{d}{2r_L \sqrt{N_{inv}}} \cong \frac{dZeB}{2E\sqrt{N_{inv}}} \simeq 2.6^\circ \left(\frac{Z}{10}\right) \frac{B_{-11} d(100 \text{ Mpc})}{E_{20} \sqrt{N_{inv}}} \quad (24)$$

Here $N_{inv} \cong d/\lambda \gtrsim 1$ is the number of inversions of the magnetic field, also expressed through the magnetic-field correlation length λ . If the two UHECRs within 3° of Cen A were accelerated by the radio jets of Centaurus A, the measured 3° deflection implies that

$$B_{-11} \gtrsim 20 \frac{(E/6 \times 10^{19} \text{ eV})}{(Z/10)}.$$

If the UHECRs originated in fact from the AGNs in the Véron-Cetty and Véron catalog [127], taking $d \cong 75$ Mpc and $\theta_d \cong 3^\circ$ gives

$$B_{-11} \gtrsim 0.9 \frac{(E/6 \times 10^{19} \text{ eV})}{(Z/10)}.$$

Both of these values are reasonable, and possibly compatible depending on gradients in the IGM field. The IGM magnetic field energy density is a small fraction of the CMBR energy density or the EBL energy density. This shows the potential power of Auger for measuring IGM fields [128]. If these IGM fields are accurate, γ -ray pulse broadening could not be measured [129].

The equation for the time delay due to the deflection of UHECRs from an impulsive source is

$$\Delta t \cong \frac{d}{6c} \theta_d^2 \simeq \frac{350 B_{-11}^2 d^3 (10 \text{ Mpc})}{N_{inv}} \left(\frac{Z}{10}\right)^2 \text{ yr} \quad (25)$$

[25, 126]. Recurrent events over decades or shorter could be observed from UHECRs powered by nearby GRBs at the distance of Cen A or GRB980425/SN1998bw ($d \cong 36$ Mpc) [130] in favorable circumstances.

Galactic Cosmic Ray Astronomy is Unlikely

It is great that Auger [15] has opened the field of extragalactic cosmic-ray astronomy, but the Pierre Auger Cosmic Ray Observatory (and its Northern Hemisphere counterpart, the Telescope Array, with half of Auger's effective area) may prove less useful for undertaking cosmic ray astronomy of galactic sources, simply because these sources are too weak.

To detect clustering in the arrival directions of signal (the definition of an astronomy), then the source distance

$$d \ll \sqrt{N_{inv}} r_L \cong 10 \sqrt{N_{inv}} \frac{E_{20}}{(Z/10) B_{\mu G}} \text{ kpc} ; \quad (26)$$

otherwise the particle trajectories would be hopelessly scrambled. To accelerate particles with energy E , equation (10), requires source luminosities

$$L \gtrsim \frac{3 \times 10^{43}}{(Z/10)^2} E_{20}^2 \text{ ergs s}^{-1} .$$

Writing this expression as a limit on particle energy gives, using eq. (26), the maximum source distance

$$d \ll 20 \frac{\sqrt{N_{inv} (L/10^{38} \text{ ergs s}^{-1})}}{B_{\mu G}} \text{ pc} \quad (27)$$

(Z drops out of the expression).

In the Milky Way, where a large scale ordered field is measured [131], probably not a large number of inversions could occur over a distance ≈ 100 pc, so I argue that N_{inv} is not large. In this case, there are not sufficiently luminous sources of nonthermal power close to the Solar system that could be observed by the cosmic rays accelerated at that source. For example, the γ -ray luminosity of Geminga, $d \cong 140$ pc, is $\approx 3 \times 10^{33}$ ergs s^{-1} [132]. The shell-type SNR RX J1713.7-3946, if 1 kpc distant, releases $\approx 10^{34}$ ergs s^{-1}

in nonthermal γ -ray energy and $\lesssim 10\times$ more in nonthermal synchrotron radiation [133]. The shell SNR RX J0852.0-4622, with $d \approx 200$ pc, releases $\approx 3 \times 10^{32}$ ergs s^{-1} [134] between 1 and 10 TeV.

This would explain the futile search for Galactic sources of cosmic rays [23, 135], which could only be detected from rare nearby SNe or hyper-energetic GRBs in our Galaxy [136, 137].

UHE Source Neutrinos from Blazars and GRBs

Discussion of neutrino production from GRBs will be kept short because it was recently reviewed [138, 139]. Our basic approach is to use measured flare nonthermal fluence to get apparent isotropic energy in the comoving frame within the uncertainty of the Doppler factor. For GRBs, we use observational constraints, including the burst rate and typical energy release, to normalize the mean (volume- and time-averaged) energy emissivity needed to power the UHECRs, from which the amount of energy that a typical GRB must release in the form of nonthermal hadrons can be derived. Our results [31] showed that for an origin of UHECRs from long-duration GRBs, with an upper SFR 3 (Figure 5), long-duration GRB blast waves must be baryon-loaded by a factor $f_{CR} \gtrsim 60$ compared to the primary electron energy that is inferred from the X/γ GRB flux.

The GRB neutrino fluences are to first order proportional to the electromagnetic X/γ radiation fluence from a GRB. Neutrino fluences expected in the collapsar GRB scenario from a burst with photon fluence $\Phi_{rad} = 3 \times 10^{-4} \text{ erg cm}^{-2}$, were calculated [140] for 3 values of the Doppler factor δ from a GRB at redshift $z = 1$ ($h = 65$). For a GRB collapsar-model calculation, we assumed that the prompt emission is contributed by $N_{spk} = 50$ spikes with characteristic timescales $t_{spk} \cong 1$ s each, which defines the characteristic size (in the proper frame) of the emitting region associated with each individual spike through the relation $R'_{spk} \cong t_{spk} \delta / (1 + z)$.

The numbers of muon neutrinos for IceCube parameters that would be detected from a single collapsar-type GRB with a baryon-loading factor $f_{CR} = 20$ for $\delta = 100, 200$ and 300 are $N_\nu =$

1.32, 0.105 and 0.016, respectively. For the large baryon load required for the proposed model of UHECRs, our calculations showed that 100 TeV – 100 PeV neutrinos could be detected several times per year from all GRBs with km-scale neutrino detectors such as IceCube [140, 31]. Detection of even 1 or 2 neutrinos from GRBs with IceCube or a northern hemisphere neutrino detector will provide compelling support for a GRB origin of UHECRs. See [138] for more details.

Detailed numerical simulations to calculate neutrino production in colliding shell scenarios of GRBs, including the diffuse neutrino intensity, are given in [141]. Calculations of neutrino fluxes during X-ray flares found with Swift was treated in [142], and neutrinos and UHECRs from low-luminosity GRBs, in [143].

Following a similar methodology and normalizing to blazar flare fluences, Armen Atayan and I [9, 68] calculated neutrino fluxes from blazars; see [144] for a recent review. We found that for equal power into ultra-relativistic electrons, which makes the X/γ emission, and protons, IceCube could detect 1 or 2 neutrinos from a powerful blazar flare like the 3C 279 flare in 1996 [78], of which GLAST should see one or two per month.

Our principle result was that FSRQs, with strong scattered radiation field, provide much more effective target photons for photopion production in their jets than do BL Lac objects. Thus powerful FSRQs like 3C 279 ($z = 0.54$), PKS 0528+134 ($z = 2.06$), CTA 102 ($z = 1.037$), of 3C 454.3 ($z = 0.86$) are a better targets for neutrino telescopes than nearby BL Lac objects.

It will be important to check these conclusions with new, incoming γ -ray data. The incredibly short flaring timescale in the TeV XBL PKS 2155-305 at $z = 0.116$ on time scales of 100s of seconds [115], with bolometric apparent γ -ray powers of $\approx 10^{45}$ ergs s^{-1} (depending on EBL assumption), represents a different regime for neutrino production in BL Lacs than considered earlier, and a probe of black holes on small size scales [145]. For blazar modeling of all types, GLAST will provide an excellent data base to determine parameters used in models for neutrino production. (see [146, 147] for blazar neutrino searches.)

Summary

Auger has already contributed three major discoveries to cosmic-ray physics:

1. the GZK cutoff, also found with HiRes;
2. Mixed ionic composition in the UHECRs up to a $few \times 10^{19}$ eV; and
3. statistical demonstration that the clustering of 27 UHECRs with energies $\gtrsim 6 \times 10^{19}$ eV follow the matter distribution as traced by nearby ($\lesssim 75$ Mpc) AGNs.

These results establish without doubt that UHECRs originate from astrophysical sources. With this information, and based on past theoretical work, I argue that GRBs and radio-loud AGNs, which are classified as blazars when viewed on-axis, are the most probable sources of UHECRs, as can be demonstrated by hadronic γ -ray signatures. The most convincing evidence would be direct detection of PeV neutrinos from UHECR sources with IceCube or KM3NET. Detection of GZK EeV neutrinos from photopion interactions of UHECRs as they propagate through EBL with an Askaryan telescope like ANITA will also importantly test astrophysical models.

In this paper, I used γ -ray observations to constrain the spectrum of the EBL between 1 and 100 μ , where it is poorly known. By adopting as a general rule, consistent with observations, that blazar $\gtrsim 100$ MeV – TeV γ -ray spectra are steeper than -2 , a low EBL, shown in Figure 9, was favored. With this EBL, we can deconvolve the intrinsic source spectrum of low-redshift sources, and calculate the photodisintegration rate of different UHECR ions. The GZK curves for different ionic species obtained with the low EBL is shown in Figure 16. These results are in accord with the location of the GZK spectral cutoff measured with Auger and HiRes, and a mixed ionic composition, because protons are more difficult to accelerate, and Fe will be broken up.

GRBs and blazars are both viable sites for UHECR acceleration, consistent with the Auger results. What will be important is to associate UHECR arrival directions with a subset of AGNs or galaxies. Small metal-poor bluish star-forming galaxies are likely hosts of long-duration GRBs [148].

Radio galaxies would host misaligned blazars, and slightly misaligned blazars could be γ -ray dim and cosmic-ray bright. GLAST will be able to see γ -ray dim AGNs (the radio galaxies M87 [149], Cen A [54], and NGC 6251 [150] are definite, likely, and probable γ -ray sources, respectively). Associating radio galaxies or GLAST γ -ray galaxies in the nearby universe with arrival directions of UHECRs could decide the question of blazar origin of the UHECRs. With the γ -ray, cosmic ray, and neutrino observations, it is likely that the problem of UHECR origin will soon be solved⁴.

Acknowledgements

I would like to thank Justin Finke, Soebur Razzaque, David Seckel, and Stefan Wagner for discussions, Guido Barbiellini for a very enjoyable talk over coffee, Alan Watson for correspondence, Armen Atoyan for collaboration, and Jeremy Holmes for his skillful coding. I would also like to thank Xiang-Yu Wang, Soebur Razzaque, and Peter Mészáros for informing me of their work prior to submission, and for a useful discussion on these issues. I am grateful to Magda González for calculating the BATSE yearly-average fluence from GRBs. I would finally like to thank the organizers, especially Alberto Carramiñana and Gustavo Medina-Tanco, for their kind invitation to the Mérida Yucatan ICRC. This work is supported by the Office of Naval Research, NASA GLAST Science Investigation DPR-S-1563-Y, and NASA *Swift* Guest Investigator Grant DPR-NNG05ED411.

References

- [1] HiRes Collaboration, ArXiv Astrophysics e-prints **0703099**, (2007).
- [2] T. Yamamoto and for the Pierre Auger Collaboration, ArXiv e-prints **707**, (2007).
- [3] K. Greisen, Physical Review Letters **16**, 748 (1966).
- [4] G. T. Zatsepin and V. A. Kuz'min, Soviet Journal of Experimental and Theoretical Physics Letters **4**, 78 (1966).
- [5] M. Unger and for the Pierre Auger Collaboration, ArXiv e-prints **706**, (2007).
- [6] M. Nagano and A. A. Watson, Reviews of Modern Physics **72**, 689 (2000).
- [7] D. F. Torres and L. A. Anchordoqui, Reports of Progress in Physics **67**, 1663 (2004).
- [8] R. Aloisio *et al.*, Astroparticle Physics **27**, 76 (2007).
- [9] A. Atoyan and C. D. Dermer, Physical Review Letters **87**, 221102 (2001).
- [10] T. Stanev *et al.*, Phys. Rev. **D62**, 093005 (2000).
- [11] M. J. Chodorowski, A. A. Zdziarski, and M. Sikora, Astrophys. J. **400**, 181 (1992).
- [12] J. L. Puget, F. W. Stecker, and J. H. Bredekamp, Astrophys. J. **205**, 638 (1976).
- [13] F. W. Stecker and M. H. Salamon, Astrophys. J. **512**, 521 (1999).
- [14] D. J. Bird *et al.*, Astrophys. J. **441**, 144 (1995).
- [15] The Pierre Auger Collaboration, Science **319**, 939 (2007).
- [16] T. Stanev *et al.*, Physical Review Letters **75**, 3056 (1995).
- [17] D. F. Torres *et al.*, Phys. Rev. **382**, 303 (2003).
- [18] E. Boldt and P. Ghosh, MNRAS **307**, 491 (1999).
- [19] F. Halzen, ArXiv e-prints **710**, (2007).
- [20] M. Ave *et al.*, Nuclear Physics B Proceedings Supplements **136**, 159 (2004).
- [21] L. A. Anchordoqui, D. Hooper, S. Sarkar, and A. M. Taylor, Astropart. Phys. **23**, 11 (2007).
- [22] A. M. Hillas, Annual Rev. Astron. Astrophys. **22**, 425 (1984).
- [23] R. U. Abbasi *et al.*, Astrophys. J. **623**, 164 (2005).
- [24] M. Vietri, Astrophys. J. **453**, 883 (1995).
- [25] E. Waxman, Physical Review Letters **75**, 386 (1995).
- [26] R. D. Preece *et al.*, Astrophys. J. Supp. **126**, 19 (2000).
- [27] D. L. Band, Astrophys. J. **578**, 806 (2002).
- [28] F. W. Stecker, Astroparticle Physics **14**, 207 (2000).

4. The theoretical basis for the results presented here are given in my book with Govind Menon entitled "High-Energy Radiation from Black Holes: γ -rays, cosmic rays, and neutrinos," to be published by Princeton University Press in 2008.

- [29] E. Liang, B. Zhang, F. Virgili, and Z. G. Dai, *Astrophys. J.* **662**, 1111 (2007).
- [30] X.-Y. Wang, S. Razzaque, P. Mészáros, and Z.-G. Dai, *Phys. Rev. D* **76**, 083009 (2007).
- [31] S. D. Wick, C. D. Dermer, and A. Atoyan, *Astroparticle Physics* **21**, 125 (2004).
- [32] P. Sreekumar *et al.*, *Astrophys. J.* **494**, 523 (1998).
- [33] A. W. Strong, I. V. Moskalenko, and O. Reimer, *Astrophys. J.* **613**, 956 (2004).
- [34] C. D. Dermer, *Astrophys. J.* **659**, 958 (2007).
- [35] J. G. Kirk and P. Duffy, *Journal of Physics G Nuclear Physics* **25**, 163 (1999).
- [36] Y. A. Gallant and A. Achterberg, *MNRAS* **305**, L6 (1999).
- [37] Y. A. Gallant, A. Achterberg, and J. G. Kirk, *Astron. Astrophys. Supp.* **138**, 549 (1999).
- [38] E. Waxman, *New Journal of Physics* **6**, 140 (2004).
- [39] C. D. Dermer and M. Humi, *Astrophys. J.* **556**, 479 (2001).
- [40] M. J. Rees and P. Mészáros, *MNRAS* **258**, 41P (1992).
- [41] M. Vietri, *Astrophys. J.* **507**, 40 (1998).
- [42] R. C. Vermeulen and M. H. Cohen, *Astrophys. J.* **430**, 467 (1994).
- [43] L. Maraschi, G. Ghisellini, and A. Celotti, *Astrophys. J. Lett.* **397**, L5 (1992).
- [44] R. Mukherjee *et al.*, *Astrophys. J.* **490**, 116 (1997).
- [45] H. Krawczynski, P. S. Coppi, and F. Aharonian, *MNRAS* **336**, 721 (2002).
- [46] S. G. Jorstad *et al.*, *Astron. J.* **130**, 1418 (2005).
- [47] F. Aharonian *et al.*, *Astrophys. J. Lett.* **664**, L71 (2007).
- [48] X.-Y. Wang, S. Razzaque, and P. Meszaros, *ArXiv e-prints* **0711**, (2007).
- [49] A. M. Beloborodov, *Astrophys. J.* **588**, 931 (2003).
- [50] C. D. Dermer, J. Chiang, and M. Böttcher, *Astrophys. J.* **513**, 656 (1999).
- [51] P. Mészáros and E. Waxman, *Physical Review Letters* **87**, 171102 (2001).
- [52] A. S. Friedman and J. S. Bloom, *Astrophys. J.* **627**, 1 (2005).
- [53] A. M. Soderberg *et al.*, *Nature* **430**, 648 (2004).
- [54] R. C. Hartman *et al.*, *Astrophys. J. Supp.* **123**, 79 (1999).
- [55] V. S. Berezinsky, P. Blasi, and V. S. Ptuskin, *Astrophys. J.* **487**, 529 (1997).
- [56] S. Inoue, G. Sigl, F. Miniati, and E. Armengaud, *ArXiv Astrophysics e-prints* (2007).
- [57] R. C. Berrington and C. D. Dermer, *ArXiv Astrophysics e-prints* (2004).
- [58] S. Inoue, G. Sigl, F. Miniati, and E. Armengaud, *ArXiv e-prints* **711**, (2007).
- [59] R. C. Berrington and C. D. Dermer, *Astrophys. J.* **594**, 709 (2003).
- [60] S. Gabici and P. Blasi, *Astrophys. J.* **583**, 695 (2003).
- [61] A. Pe’er *et al.*, *Astrophys. J. Lett.* **664**, L1 (2007).
- [62] K. Hurley *et al.*, *Nature* **372**, 652 (1994).
- [63] M. Böttcher and C. D. Dermer, *Astrophys. J. Lett.* **499**, L131 (1998).
- [64] M. Sommer *et al.*, *Astrophys. J. Lett.* **422**, L63 (1994).
- [65] M. M. González *et al.*, *Nature* **424**, 749 (2003).
- [66] A. Pe’er and E. Waxman, *Astrophys. J. Lett.* **603**, L1 (2004).
- [67] C. D. Dermer and A. Atoyan, *Astron. Astrophys.* **418**, L5 (2004).
- [68] A. M. Atoyan and C. D. Dermer, *Astrophys. J.* **586**, 79 (2003).
- [69] C. D. Dermer, *Astrophys. J.* **664**, 384 (2007).
- [70] G. Tagliaferri *et al.*, *Nature* **436**, 985 (2005).
- [71] J. P. Rachen and P. Mészáros, *Phys. Rev. D* **58**, 123005 (1998).
- [72] B. Zhang *et al.*, *Astrophys. J.* **642**, 354 (2006).
- [73] H. Krawczynski *et al.*, *Astrophys. J.* **601**, 151 (2004).
- [74] M. Böttcher, *Astrophys. J.* **621**, 176 (2005).
- [75] A. Reimer, M. Böttcher, and S. Postnikov, *Astrophys. J.* **630**, 186 (2005).
- [76] S. Razzaque, P. Mészáros, and B. Zhang, *Astrophys. J.* **613**, 1072 (2004).
- [77] C. D. Dermer, E. Ramirez-Ruiz, and T. Le, *Astrophys. J. Lett.* **664**, L67 (2007).
- [78] A. E. Wehrle *et al.*, *Astrophys. J.* **497**, 178 (1998).
- [79] R. C. Hartman *et al.*, *Astrophys. J.* **553**, 683 (2001).
- [80] M. Teshima *et al.*, *ArXiv e-prints* **709**, (2007).

- [81] C. D. Dermer, *Astrophys. J.***574**, 65 (2002).
- [82] A. M. Hopkins and J. F. Beacom, *Astrophys. J.***651**, 142 (2006).
- [83] V. S. Berezhinskii and S. I. Grigor'eva, *Astron. Astrophys.***199**, 1 (1988).
- [84] T. Le and C. D. Dermer, *Astrophys. J.***661**, 394 (2007).
- [85] V. Berezhinsky, A. Gazizov, and S. Grigorieva, *Phys. Rev. D***74**, 043005 (2006).
- [86] V. Berezhinsky, *Journal of Physics Conference Series* **47**, 142 (2006).
- [87] S. W. Barwick *et al.*, *Physical Review Letters* **96**, 171101 (2006).
- [88] S. W. Barwick, *ArXiv Astrophysics e-prints* (2006).
- [89] A. Karle *et al.*, *Nuclear Physics B Proceedings Supplements* **118**, 388 (2003).
- [90] K. Mannheim and P. L. Biermann, *Astron. Astrophys.***253**, L21 (1992).
- [91] D. E. Harris and H. Krawczynski, *Annual Rev. Astron. Astrophys.* **44**, 463 (2006).
- [92] A. Atoyan and C. D. Dermer, *Astrophys. J.***613**, 151 (2004).
- [93] S. G. Jorstad *et al.*, *Astrophys. J.***556**, 738 (2001).
- [94] A. Lähteenmäki and E. Valtaoja, *Astrophys. J.***590**, 95 (2003).
- [95] C. M. Urry and P. Padovani, *Proc. Astron. Soc. Pacific***107**, 803 (1995).
- [96] A.-C. Donea and R. J. Protheroe, *Astroparticle Physics* **18**, 377 (2003).
- [97] M. Boettcher and C. D. Dermer, *Astron. Astrophys.***302**, 37 (1995).
- [98] R. D. Blandford and A. Levinson, *Astrophys. J.***441**, 79 (1995).
- [99] C. von Montigny *et al.*, *Astrophys. J.***483**, 161 (1997).
- [100] E. Pian *et al.*, *Astrophys. J.***521**, 112 (1999).
- [101] L. A. Anchordoqui *et al.*, *Phys. Rev. D***75**, 063001 (2007).
- [102] H. Netzer *et al.*, *Active Galactic Nuclei* (Saas-Fee Advanced Course 20. Lecture Notes 1990. Swiss Society for Astrophysics and Astronomy, XII, 280 pp. 97 figs.. Springer-Verlag Berlin Heidelberg New York, Saas-Fee, 1990).
- [103] S. Kaspi and H. Netzer, *Astrophys. J.***524**, 71 (1999).
- [104] H. T. Liu and J. M. Bai, *Astrophys. J.***653**, 1089 (2006).
- [105] A. Reimer, *Astrophys. J.***665**, 1023 (2007).
- [106] M. G. Hauser and E. Dwek, *Annual Rev. Astron. Astrophys.* **39**, 249 (2001).
- [107] F. W. Stecker, M. G. Baring, and E. J. Summerlin, *Astrophys. J. Lett.***667**, L29 (2007).
- [108] F. W. Stecker and O. C. de Jager, *Astrophys. J.***476**, 712 (1997).
- [109] D. B. Sanders and I. F. Mirabel, *Annual Rev. Astron. Astrophys.* **34**, 749 (1996).
- [110] C. D. Dermer, J. Bland-Hawthorn, J. Chiang, and K. McNaron-Brown, *Astrophys. J. Lett.***484**, L121 (1997).
- [111] M. Obrić *et al.*, *MNRAS***370**, 1677 (2006).
- [112] D. A. Dale *et al.*, *Astrophys. J.***655**, 863 (2007).
- [113] I. V. Moskalenko, T. A. Porter, and A. W. Strong, *Astrophys. J. Lett.***640**, L155 (2006).
- [114] F. Aharonian *et al.*, *Astron. Astrophys.***470**, 475 (2007).
- [115] W. Benbow *et al.*, *ArXiv e-prints* **709**, (2007).
- [116] D. Mazin and M. Raue, *Astron. Astrophys.***471**, 439 (2007).
- [117] T. M. Kneiske, T. Bretz, K. Mannheim, and D. H. Hartmann, *Astron. Astrophys.***413**, 807 (2004).
- [118] F. Aharonian *et al.*, *Nature***440**, 1018 (2006).
- [119] J. R. Primack, J. S. Bullock, and R. S. Somerville, in *High Energy Gamma-Ray Astronomy*, Vol. 745 of *American Institute of Physics Conference Series*, edited by F. A. Aharonian, H. J. Völk, and D. Horns (AIP, New York, 2005), pp. 23–33.
- [120] F. W. Stecker, *ArXiv e-prints* **709**, (2007).
- [121] M. A. Malkan and F. W. Stecker, *Astrophys. J.***496**, 13 (1998).
- [122] M. A. Malkan and F. W. Stecker, *Astrophys. J.***555**, 641 (2001).
- [123] R. J. Gould and G. P. Schröder, *Physical Review* **155**, 1408 (1967).
- [124] G. G. Fazio and F. W. Stecker, *Nature***226**, 135 (1970).
- [125] E. Orlando and A. W. Strong, *Astrophys. Space Sci.***309**, 359 (2007).
- [126] E. Waxman and P. Coppi, *Astrophys. J. Lett.***464**, L75 (1996).
- [127] M.-P. Véron-Cetty and P. Véron, *Astron. Astrophys.***455**, 773 (2006).

- [128] P. P. Kronberg, in *American Institute of Physics Conference Series*, Vol. 558 of *American Institute of Physics Conference Series*, edited by F. A. Aharonian and H. J. Völk (AIP, New York, 2001), pp. 451–462.
- [129] R. Plaga, *Nature***374**, 430 (1995).
- [130] S. Foley *et al.*, *Astron. Astrophys.***447**, 891 (2006).
- [131] M. J. Reid, K. M. Menten, and A. L. Argon, The Origins of Galactic Magnetic Fields, 24th meeting of the IAU, Joint Discussion 14, August 2000, Manchester, England, meeting abstract. **14**, (2000).
- [132] M. P. Ulmer, *Astrophys. J. Supp.***90**, 789 (1994).
- [133] F. Aharonian *et al.*, *Astron. Astrophys.***449**, 223 (2006).
- [134] H. E. S. S. Collaboration: M. Lemoine-Goumard *et al.*, *ArXiv e-prints* **709**, (2007).
- [135] The Pierre AUGER Collaboration, *Astroparticle Physics* **27**, 244 (2007).
- [136] P. L. Biermann, G. Medina Tanco, R. Engel, and G. Pugliese, *Astrophys. J. Lett.***604**, L29 (2004).
- [137] C. D. Dermer and J. M. Holmes, *Astrophys. J. Lett.***628**, L21 (2005).
- [138] C. D. Dermer and A. Atoyan, *New Journal of Physics* **8**, 122 (2006).
- [139] P. Mészáros and S. Razzaque, *ArXiv Astrophysics e-prints* (2006).
- [140] C. D. Dermer and A. Atoyan, *Physical Review Letters* **91**, 071102 (2003).
- [141] K. Murase and S. Nagataki, *Phys. Rev. D***73**, 063002 (2006).
- [142] K. Murase and S. Nagataki, *Physical Review Letters* **97**, 051101 (2006).
- [143] K. Murase, K. Ioka, S. Nagataki, and T. Nakamura, *Astrophys. J. Lett.***651**, L5 (2006).
- [144] A. Levinson, *International Journal of Modern Physics A* **21**, 6015 (2006).
- [145] M. C. Begelman, A. C. Fabian, and M. J. Rees, *ArXiv e-prints* **709**, (2007).
- [146] J. K. Becker *et al.*, *Astroparticle Physics* **28**, 98 (2007).
- [147] M. Ackermann, *Astrophys. Space Sci.***309**, 421 (2007).
- [148] E. Le Floc'h *et al.*, *Astron. Astrophys.***400**, 499 (2003).
- [149] M. Beilicke *et al.*, in *American Institute of Physics Conference Series*, Vol. 921 of *American Institute of Physics Conference Series*, edited by S. Ritz, P. Michelson, and C. A. Meegan (AIP, New York, 2007), pp. 147–149.
- [150] R. Mukherjee, J. Halpern, N. Mirabal, and E. V. Gotthelf, *Astrophys. J.***574**, 693 (2002).